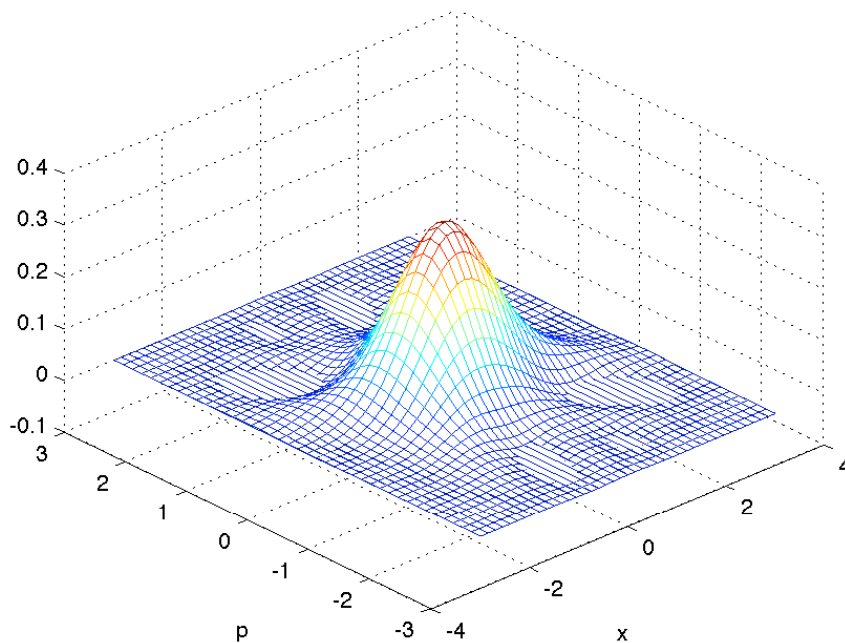




Production of a squeezed state of light



A bachelor thesis by:

Thomas Aktor,

Stefan L. Christensen

and William H. P. Nielsen

Academic supervisor: Eugene S. Polzik

May 2009.

Statement

The authors hereby confirm that this project is the result of a team effort where everyone has contributed equally.

Thomas Aktor May 29, 2009

Stefan L. Christensen May 29, 2009

William H. P. Nielsen May 29, 2009

Acknowledgements

This thesis is a product of the work done at QUANTOP from November 2008 to the end of May 2009. It has been half a year, in which most of the time was spent in the lab; turning, building, cleaning and measuring. This work was, although frustrating at times, a very realistic introduction to the world of experimental quantum optics. Results are available, but not without dedicated labour. The bitter the grapes, the sweeter the taste of the wine.

Starting out as a novice in the field of experimental quantum optics, we would surely not have made it this far if it had not been for the help of a number of people. Especially, we want to thank Bo Melholt Nielsen for taking good care of us, be it answering questions or sharing his substantial knowledge in the lab. His patience has been remarkable. We would also like to thank Kasper Jensen, for babysitting us when Bo was babysitting his newborn daughter, and Koji Usami for advise and help in the lab. Of course, none of this would ever have amounted to anything, if not Eugene Polzik had kindly given us the opportunity to work at QUANTOP, an opportunity we appreciate. And last but not least, we thank the rest of the QUANTOP gang for sharing coffee, cake and most importantly for always keeping their office doors open and being eager to help us out.

Abstract

Vi har i dette bachelorprojekt beskæftiget os med lystilstande der er klemte i kvadraturerne, dvs. har formindskede fluktuationer i forhold til standardkvantegrænsen sat af vacuum, og hvorledes disse kan frembringes eksperimentelt. Disse lystilstande betragtes som værende distinkt kvantemekaniske eller ikke-klassiske, og er af stor interesse indenfor kvanteoptik og kvanteoptiske virkeliggørelser af kvanteinformativ kredsløb.

I dette projekt introducerer vi disse tilstande og forklarer hvorledes de kan beskrives gennem eksempelvis en kvasisandsynlighedsfordeling ved navn Wigner-funktionen. Hovedvægten er dog lagt på hvorledes disse tilstande bliver skabt i laboratoriet og hvorledes man kan måle dem. Eftersom den eksperimentielle opstilling brugt til at fremstille disse tilstande er ganske indviklet, vil vi i særdeleshed fokusere på underprocessen frekvensfordobling, hvori lys sendes gennem et ikke-linært krystal og derved frembringer lys af den halve bølgelængde. Denne proces er beskrevet både teoretisk og eksperimentielt, og vi har grundigt karakteriseret den i forsøget benyttede frekvensfordobler igennem målinger af bl.a. dens omdannelseseffektivitet og finesse.

Efter denne gennemgang præsenterer vi de af det klemte lys målte data, der viser at klemningen er lykkedes. Disse data præsenteres på flere måder, herunder hører en ikke-triviel proces med at genskabe den målte kvantetilstand ud fra de tilstandsreducerende målinger.

Contents

1	Preface/Introduction	1
1.1	Introduction	1
2	General quantum optical theory	2
2.1	States of light and their representation	2
2.1.1	Field operators.	2
2.1.2	Fock states	3
2.1.3	Coherent states	4
2.1.4	Density operator	4
2.1.5	Quantum optical phase-space	5
2.1.6	Quasiprobability distributions	5
2.1.7	Squeezed States.	6
2.2	Quantum tomography	8
2.2.1	Balanced homodyne detection	8
2.2.2	Maximum likelihood algorithm	10
3	The experiment	12
3.1	Design of the experiment	12
3.2	Laser and the laser light	13
3.2.1	Incoupling 1: The Gaussian beam	13
3.2.2	Incoupling 2: Propagation through optical elements	15
3.2.3	Measuring the q parameter	15
3.2.4	Japanese Swinging Stick	17
3.3	SHG	18
3.3.1	Outline	18
3.3.2	Phase matching	18
3.3.3	Optimal waist	20
3.3.4	Cavity	21
3.3.5	Characterizing the SHG	22
3.4	OPO	25
3.5	Homodyne detection	25
3.6	Data presentation	27
3.6.1	Phase calibration	27
3.6.2	Seeing is believing	27
3.6.3	Reconstructed quantum state	28
4	Summary and outlook	31
4.1	Summary	31
4.2	Outlook	31
	Bibliography	31

A	The error function	a
B	Lorentz model of SHG	c
B.1	Nonlinear material	c
C	Derivation of the Gaussian beam	e
C.1	The paraxial wave equation	e

Chapter 1

Preface/Introduction

1.1 Introduction

In [5] it is stated in the introduction that "[Quantum optics] is a field which attracts the brightest students at present". Even though the authors of this thesis obviously cannot live up to such a label, the remark has been very inspiring to us. For it is indeed true that the field of quantum optics contains a wide range of attractions, and that brightness is often required to understand them. What has attracted us the most is the opportunity of, through dedicated labour, to obtain a first-hand impression of quantum mechanical systems.

In this thesis we shall be dealing with the phenomenon of *squeezing*. More specifically, what we shall squeeze is the noise of light, hence reducing it below its normal value. The strangeness of squeezing becomes evident as one realizes that squeezing can even be applied to vacuum, making it somehow less noisy than ordinary vacuum. This is indeed manipulation of nature at a very deep level, and a highly astonishing effect. What is maybe more astonishing is the broad range of applications of squeezed light and vacuum. For instance, one can use this very quiet light to improve the precision of measurements, [14]. Also, since squeezed states of light are considered to be non-classical (i.e. truly quantum mechanical), they are a powerful benchmarking tool for testing whether a so-called quantum memory really deserves the label 'quantum', one simply asks: can this memory store and recall a squeezed state? At Quantop, other experiments are doing just this, writing different light states to cesium atoms, using light resonant with the $6S_{1/2} \rightarrow 6P_{3/2}$ transition [10, Page 76].

In this thesis we will present an overview of an experiment producing squeezed light. Since a full description of such an experiment and the theory underlying it would require (at least) a master's thesis, we have had to skip many details and parts of the experiment. We have chosen to focus our attention on the second harmonic generator and the process of quantum state reconstruction, with a strong emphasis on actual experimental obstacles and how to overcome them. We did not want to simply read about the experiment and then re-present what we had read, but rather get an actual *hands-on* feeling for the equipment. Hopefully, some of this know-how will be transmitted to the reader.

The thesis is divided into three main parts. First, we give the minimal quantum optical theory of squeezing and of quantum optical measurement needed to understand the experiment. Then, we proceed to give a brief overview of the experiment, followed by a careful explanation of the second harmonic generator, including theory and measured data as this becomes necessary. Finally, the squeezed light data is analysed and presented, and a noise reduction (darkness quieting) of around 2dB is seen.

Chapter 2

General quantum optical theory

In this section we shall give a short introduction to quantum optics. The aim is to briefly sketch the background of squeezing, such that readers familiar with quantum mechanics will be able to understand the theory of squeezed states. For a general and much more rigorous derivation of the following we refer to [5] and [7], on which this treatment is based.

2.1 States of light and their representation

2.1.1 Field operators.

We postulate that a light field of frequency ω is governed by the quantum mechanical harmonic oscillator with the Hamiltonian [5, Chapter 2].

$$\hat{\mathcal{H}} = \hbar\omega \left(\hat{a}^\dagger \hat{a} - \frac{1}{2} \right), \quad (2.1.1)$$

where \hat{a} is the annihilation operator and \hat{a}^\dagger is the creation operator. They obey the bosonic commutator relation

$$[\hat{a}, \hat{a}^\dagger] = 1, \quad (2.1.2)$$

and are obviously not Hermitian. The Hermitian combination of creation and annihilation operators, $\hat{a}^\dagger \hat{a}$, that appears in the Hamiltonian is also known as the photon number operator, and sometimes denoted by \hat{n} , i.e.,

$$\hat{n} \equiv \hat{a}^\dagger \hat{a}. \quad (2.1.3)$$

As always, we prefer to work with Hermitian and hence observable operators. Two Hermitian operators one often stumbles upon are the quadrature operators, \hat{q} and \hat{p} , given by¹

$$\hat{q} = \frac{1}{\sqrt{2}} (\hat{a} + \hat{a}^\dagger), \quad \hat{p} = \frac{1}{i\sqrt{2}} (\hat{a} - \hat{a}^\dagger). \quad (2.1.4)$$

The commutator between the two quadrature operators is

$$[\hat{q}, \hat{p}] = i, \quad (2.1.5)$$

as can easily be checked. For convenience we have set $\hbar = 1$, which can always be achieved by a proper rescaling of the units. Due to the canonical commutator

¹We alert the reader that a variety of operators with the names *quadrature operators* appear in the literature, all differing by factors of 2, $\sqrt{2}$ and so on, depending on choice of normalization and the value of \hbar . We use the definition from [7].

relation between \hat{q} and \hat{p} , these operators can be interpreted as a set of canonical position and momentum variables for the electromagnetic harmonic oscillator, justifying the notation used. For further use it is convenient to introduce the generalized quadrature operator

$$\hat{q}_\theta = \hat{q} \cos \theta + \hat{p} \sin \theta, \quad \text{obeying} \quad [\hat{q}_\theta, \hat{q}_\phi] = [\hat{q}, \hat{p}] \sin(\phi - \theta). \quad (2.1.6)$$

We note that $\hat{q}_0 = \hat{q}$ and $\hat{q}_{\pi/2} = \hat{p}$. It will be shown in Section 2.2.1 that the generalized quadrature is exactly the quantity we are measuring in the experiment. Before we can give a complete description of squeezed states, we, as always, need to address the question regarding which basis we should work in.

2.1.2 Fock states

In elementary quantum mechanics one makes the acquaintance² of the energy eigenstates of the harmonic oscillator Hamiltonian,

$$\hat{\mathcal{H}}|n\rangle = E_n|n\rangle, \quad \hat{n}|n\rangle = n|n\rangle. \quad (2.1.7)$$

They have the well-known properties that

$$\begin{aligned} \hat{a}|n\rangle &= \sqrt{n}|n-1\rangle \\ \hat{a}^\dagger|n\rangle &= \sqrt{n+1}|n+1\rangle \end{aligned} \quad (2.1.8)$$

and are of course chosen to be an orthonormal basis of the Hilbert space for the light field. In quantum optics, they usually go by the name of the Fock or number states. We recall that any number state can be constructed by subsequent application of the creation operator to the vacuum³ state, $|0\rangle$, as

$$|n\rangle = \frac{\hat{a}^{\dagger n}}{\sqrt{n!}}|0\rangle. \quad (2.1.9)$$

We will be dealing substantially with the fluctuations of light states, and therefore address their variances. The variance of an operator, \hat{A} , is given as

$$(\Delta\hat{A})^2 = \langle \hat{A}^2 \rangle - \langle \hat{A} \rangle^2. \quad (2.1.10)$$

Considering the quadrature operators and working in the Fock basis, by using equation (2.1.8) and the commutator between \hat{a} and \hat{a}^\dagger , we find for any number state that

$$\begin{aligned} \langle \hat{p}^2 \rangle &= \langle n|\hat{p}|n\rangle = \frac{1}{2}(2n+1) \\ \langle \hat{p} \rangle^2 &= \langle n|\hat{p}|n\rangle^2 = 0, \end{aligned} \quad (2.1.11)$$

which also holds for \hat{q} and in fact any normalized linear combination of the two, i.e. \hat{q}_θ for any θ . The variances in the quadratures are then given as

$$(\Delta\hat{q})^2 = (\Delta\hat{p})^2 = (\Delta\hat{q}_\theta)^2 = \frac{1}{2}(2n+1). \quad (2.1.12)$$

An interesting point is that even the vacuum, $n = 0$, has fluctuations. The magnitude of these fluctuations are known as the standard quantum limit of uncertainty (SQL), for rather obvious reasons. The goal of our experiment will be to break this limit by producing a state with fluctuations of lesser magnitude than the SQL.

²See any introductory book on quantum mechanics.

³Vacuum is in this thesis equivalent to a light state with no photons.

2.1.3 Coherent states

We now introduce another set of quantum optical states, the coherent states, denoted $|\alpha\rangle$. One way to define them is as eigenkets of the annihilation operator

$$\hat{a}|\alpha\rangle = \alpha|\alpha\rangle, \quad (2.1.13)$$

where α in general is a complex number since \hat{a} is a non-Hermitian operator. Using the fact that the Fock states form a complete set, we can expand the coherent states in this basis and find

$$|\alpha\rangle = \exp\left[-\frac{1}{2}|\alpha|^2\right] \sum_{n=0}^{\infty} \frac{\alpha^n}{\sqrt{n!}} |n\rangle. \quad (2.1.14)$$

A different way to define⁴ these states is as displaced vacuum states (see Figure 2.1 for an intuitive picture)

$$|\alpha\rangle = \hat{D}(\alpha)|0\rangle, \quad (2.1.15)$$

where the displacement operator, $\hat{D}(\alpha)$, is given as

$$\hat{D}(\alpha) = \exp[\alpha\hat{a}^\dagger - \alpha^*\hat{a}]. \quad (2.1.16)$$

This definition implies that coherent states have the same fluctuations as the vacuum state. It can be shown, see [5, Section 3.2], that this definition, upon expanding in the Fock basis, will also yield equation (2.1.14), making the two definitions equivalent.

2.1.4 Density operator

Once we have chosen the state kets we prefer for the description of our light, no one can guarantee us that the light field will be in a pure ensemble⁵ of one of these states. On the contrary, the system will, in real life, be in a statistical mixture of states. To each state $|\alpha_i\rangle$ in the ensemble we thus associate a fractional probability of finding the system in that particular state. We denote this fractional probability by w_i and demand that the following normalization condition holds:

$$\sum_i w_i = 1. \quad (2.1.17)$$

The density operator is now readily defined as

$$\hat{\rho} \equiv \sum_i w_i |\alpha_i\rangle\langle\alpha_i|. \quad (2.1.18)$$

From the basis independency of the trace and equation (2.1.17) it is clear that

$$\text{Tr}(\hat{\rho}) = 1. \quad (2.1.19)$$

It should be noted that all the physical properties of a given ensemble are completely contained in the density operator. One particularly nice feature shown in [16, Section 3.4] is that the expectation value of an operator \hat{A} can be calculated as

$$\langle\hat{A}\rangle = \text{Tr}(\hat{\rho}\hat{A}). \quad (2.1.20)$$

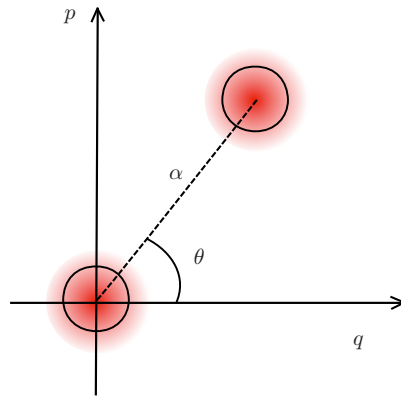


Figure 2.1: A vacuum state, $\alpha = 0$, and a coherent state. Since α is complex, we sometimes write $\alpha = |\alpha|e^{i\theta}$.

2.1.5 Quantum optical phase-space

Although the concept of a quantum mechanical phase-space is essentially flawed by the fact that \hat{q} and \hat{p} are incompatible observables, it is customary and of great advantage to introduce phase-space representations of the light states anyway. Some care should be taken in doing this, and we will stress the differences between the classical and the quantum optical phase-spaces as they appear.

First of all, the inherent uncertainty in the quadratures makes the notion of points in phase-space completely pointless. Whereas a system in classical physics is described by a point in phase-space, we must consider the system to occupy some finite region. If we for instance consider a coherent state with amplitude α , then

$$\begin{aligned} \langle \hat{q} \rangle &= \sqrt{2}\text{Re}(\alpha), & \Delta \hat{q} &= \frac{1}{\sqrt{2}} \\ \langle \hat{p} \rangle &= \sqrt{2}\text{Im}(\alpha), & \Delta \hat{p} &= \frac{1}{\sqrt{2}}. \end{aligned}$$

This gives rise to the rather intuitive phase-space picture of a coherent state shown in Figure 2.1. A useful connection to the generalized quadrature operator is the notion that $\alpha = \langle q_\theta \rangle e^{i\theta}$.

It should be clear that measurements of the quadratures performed on the system will somehow "draw" results from within the shaded regions in Figure 2.1. A more quantitative definition of this "somehow" is the aim of the next section.

2.1.6 Quasiprobability distributions

In analogy with classical optics we will seek a phase-space representation of a quantum mechanical state of light. What we in particular are interested in is a phase space probability distribution, i.e., a mapping from the complex plane (the phase-space) into the real numbers ((quasi)probability of obtaining these quadrature values). A multitude of these functions exists⁶, but we will only be interested in the so-called Wigner function.

There are many ways to enter the discussion of the Wigner function, $W(q, p)$. Here we follow [7, Section 3.1.1], where the Wigner function is defined by postulating

⁴They can also be defined as minimum uncertainty states, see [5, Section 3.1].

⁵As defined in [16, Section 3.4].

⁶We refer the reader to [6].

it's properties. It turns out that all we need is to demand is the right marginal distributions

$$\int W(q \cos \theta - p \sin \theta, q \sin \theta + p \cos \theta) dp = |\psi(q_\theta)|^2 = \text{pr}(q, \theta), \quad (2.1.21)$$

i.e., that the marginal distributions are the probability distributions of the orthogonal quadrature operators. Note that these distributions are actual (not quasi) and directly measurable probability distributions, and they are indeed the distributions we will sample in our experiment. Skipping the calculation given in [7] this will yield the Wigner function given by

$$W(q, p) = \frac{1}{2\pi} \int \exp(ipx) \left\langle q - \frac{x}{2} | \hat{\rho} | q + \frac{x}{2} \right\rangle dx, \quad (2.1.22)$$

where $|q \pm \frac{x}{2}\rangle$ are eigenstates of the position operator. It can in general be shown [7, Section 3.1.2] that

$$|W(q, p)| \leq \frac{1}{\pi}, \quad (2.1.23)$$

which is of course not allowable for a classical probability distribution. Hence the name *quasi*probability distribution. The negativeness of the Wigner function can be taken as a measure of non-classicality⁷. In this thesis we will use the term of non-classicality as in [5, Chapter 7].

2.1.7 Squeezed States.

In general, the Heisenberg uncertainty relation for two operators whose commutator is

$$[\hat{A}, \hat{B}] = i\hat{C}, \quad (2.1.24)$$

can be expressed as [5, Section 7.1]

$$\langle (\Delta\hat{A})^2 \rangle \langle (\Delta\hat{B})^2 \rangle \geq \frac{1}{4} |\langle \hat{C} \rangle|^2. \quad (2.1.25)$$

We call a state squeezed if either

$$\langle (\Delta\hat{A})^2 \rangle < \frac{1}{2} |\langle \hat{C} \rangle| \quad \text{or} \quad \langle (\Delta\hat{B})^2 \rangle < \frac{1}{2} |\langle \hat{C} \rangle|. \quad (2.1.26)$$

In the following, we shall only consider squeezing in the quadrature operators⁸. Using the commutator of equation (2.1.5), we have squeezing if

$$\langle (\Delta\hat{q})^2 \rangle < \frac{1}{2} \quad \text{or} \quad \langle (\Delta\hat{p})^2 \rangle < \frac{1}{2}. \quad (2.1.27)$$

From Heisenberg's uncertainty relation, squeezing in \hat{q} will raise the variance in \hat{p} by the at least the same amount. The obvious question to ask is how this is accomplished. For this purpose we introduce the squeezing operator as

$$\hat{S}(\xi) \equiv \exp \left[\frac{1}{2} (\xi^* \hat{a}^2 - \xi \hat{a}^{\dagger 2}) \right], \quad (2.1.28)$$

where we have introduced the squeezing parameter $\xi = \zeta e^{i\phi}$. We allow the squeezing parameter to be complex, in order to account for squeezing along any axis in

⁷As was described in the introduction, it is very important for quantum memories to be able to distinguish between classical and non-classical light states.

⁸Throughout this paper squeezing will be understood to mean quadrature squeezing.

phase space⁹. The correspondence to the displacement operator given in equation (2.1.16) is clear, the main difference being the squaring of the creation and annihilation operators in the squeezing operator. This is the first hint that photons in a squeezed state are created and annihilated in pairs, yielding a somewhat special photon distribution. The squeezing operator gives the squeezed vacuum as

$$|\xi\rangle = \hat{S}(\xi)|0\rangle. \quad (2.1.29)$$

It can be shown in several ways that this operator has the desired action. We find, in accordance with [7, Section 2.3], that

$$(\Delta\hat{p})^2 = \frac{1}{2}e^{-2\zeta}, \quad \text{and} \quad (\Delta\hat{q})^2 = \frac{1}{2}e^{+2\zeta}. \quad (2.1.30)$$

The question is now how we can produce a squeezed state in the laboratory. More specifically, we will seek an interaction Hamiltonian such that the time evolution governed by this Hamiltonian will yield the squeezing operator of equation (2.1.28). Expressed in formula,

$$\hat{U}(t, t_0) = \exp(-i\hat{\mathcal{H}}_I(t - t_0)/\hbar) = \hat{S}(\xi). \quad (2.1.31)$$

Dipping into mother nature's great variety of Hamiltonians, we find that the process of *degenerate parametric down-conversion* has the desired form. This is a nonlinear process in which a photon at a frequency ω is converted in a crystal into two photons at frequencies $\omega/2$, which will be described in greater detail in section 3.4. In the parametric approximation, the Hamiltonian of this process is given by [5, Section 7.3]

$$\hat{\mathcal{H}}_I = i\hbar(\kappa^*\hat{a}^2 - \kappa\hat{a}^{\dagger 2}), \quad (2.1.32)$$

where κ is a parameter related to the second-order nonlinear susceptibility χ of the crystal used and the amplitude β of the pump field by $\kappa = \beta\chi$. It is now an elementary task to see that equation (2.1.31) holds for $\xi = 2\kappa(t - t_0)$.

Having defined the effect of squeezing and how to achieve it, we are now ready to look at some of the properties of squeezed states. First off all, we want a representation of the squeezed vacuum state in terms of the Fock states;

$$|\xi\rangle = \sum_{n=0}^{\infty} C_n |n\rangle. \quad (2.1.33)$$

We will drop the lengthy calculation of determining the expansion coefficients and instead refer to [5, Section 2.3]. With these coefficients one easily finds the probability of detecting m photons in the field as being

$$P_m = |C_m|^2 = \begin{cases} 0 & \text{for } m \text{ odd} \\ \frac{(2m)!}{2^{2m}(m!)^2} \frac{(\tanh(\zeta))^{2m}}{\cosh \zeta} & \text{for } m \text{ even.} \end{cases} \quad (2.1.34)$$

Thus, as it was expected, we are only detecting pairs of photons¹⁰ as is also seen in Figure 2.2.

As was the case for the coherent states, we have an intuitively clear representation of a squeezed coherent state in phase space. Since the variance is squeezed in one quadrature and thus increased in the other, it is obvious that circles will become ellipses, see Figure 2.3(a). The same is seen when plotting the Wigner function in Figure 2.3(b). It is exactly this Wigner function we will reconstruct using homodyne detection and state tomography. Knowledge of the photon distribution for squeezed vacuum will be important in this connection.

⁹Note that no measurable absolute angle exists in quantum optical phase space, [5, Section 2.7].

¹⁰We only have even photon numbers since we want the vacuum state to be included in the solution.

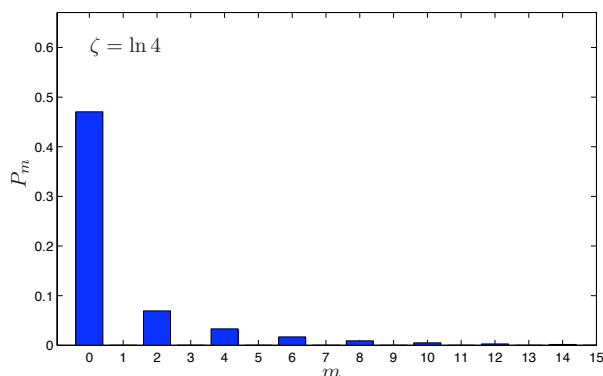


Figure 2.2: Theoretically generated histogram of photon number distribution for squeezed vacuum.

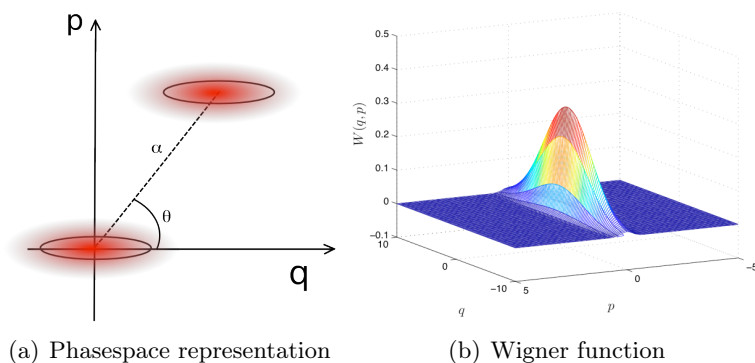


Figure 2.3: Two dimensional phasespace and Wigner function for a coherent state squeezed in \hat{p} -quadrature.

2.2 Quantum tomography

In this section, we shall consider the problem of measuring and afterwards, by quantum state tomography, reconstructing a density matrix and Wigner function from the measured data. We recall that we are dealing with quadrature squeezed light, and that we therefore, in order to determine whether a state is squeezed or not, must be able to detect the variance in the quadrature operator.

2.2.1 Balanced homodyne detection

The method of balanced homodyne detection is a standard measurement procedure employed all over the field of experimental quantum optics [7]. The experimental setup required for homodyne detection consists of a beam splitter and two photodetectors. We start by discussing the quantum mechanical action of a beam splitter described¹¹ by [12, Section 2.5]

$$\begin{bmatrix} \hat{a}_2 \\ \hat{a}_3 \end{bmatrix} = \begin{bmatrix} t & -r \\ r & t \end{bmatrix} \begin{bmatrix} \hat{a}_0 \\ \hat{a}_1 \end{bmatrix}, \quad |t|^2 + |r|^2 = 1. \quad (2.2.1)$$

The notion of the homodyne detection being *balanced*, refers to the fact that the output intensities are of equal magnitude, i.e. the beamsplitter should transform the

¹¹With the small difference that we, as in [5], allow t and r to be complex.

operators according to

$$\hat{a}_2 = \frac{1}{\sqrt{2}}(\hat{a}_0 + i\hat{a}_1), \quad \hat{a}_3 = \frac{1}{\sqrt{2}}(i\hat{a}_0 + \hat{a}_1). \quad (2.2.2)$$

Such a beam splitter is called a 50:50 beam splitter, for obvious reasons. We note that all ports must be accounted for, even if one of them only contains the vacuum state. This is due to the fact that a vacuum state has fluctuations as discussed in Section 2.1.2, and that the transformation will be affected by these fluctuations¹² [5, Section 6.2]. Besides that, the beam splitter works in a very intuitive way, mixing the two input states into two output states.

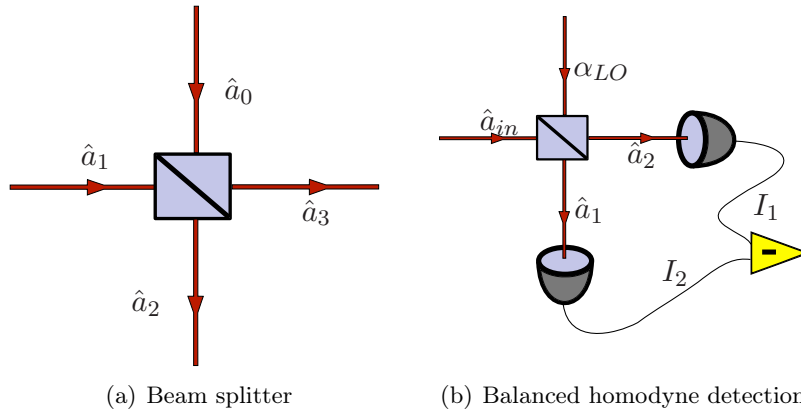


Figure 2.4: A beam splitter and its use in homodyne detection. Note the classical input in (b).

The setup for balanced homodyne detection is shown in Figure 2.4(b). The main idea in homodyne detection is 'mixing up' the quantum fluctuations of a weak signal with a strong classical reference field of the same frequency, thus making the quantum fluctuations visible. This is readily achieved experimentally by splitting the original master laser beam into two parts, using one of these as input for the squeezing apparatus, and the other one as the reference field, or, as we will call it, the *local oscillator*, and then combining the two once more using a 50:50 beam splitter.

As the two beams propagate along different optical paths, they will get out of phase with one another. Since only their relative phase difference, θ , matters (we assume the frequency to be fixed once and for all), we may absorb it into the complex amplitude of the local oscillator by taking $\alpha_{LO} = |\alpha_{LO}|e^{i\theta}$. The transformation then yields the outputs

$$\hat{a}_1 = (|\alpha_{LO}|e^{i\theta} + i\hat{a}_{in}), \quad \hat{a}_2 = (i|\alpha_{LO}|e^{i\theta} + \hat{a}_{in}). \quad (2.2.3)$$

If we are dealing with linear response photodiodes, the measured intensity (rather: measured current which is proportional to intensity) will be proportional to the mean photon number in each arm of the setup. By subtracting the two measured intensities, we can thus acquire a number, I_- , fulfilling

$$I_- = I_2 - I_1 \propto \langle \hat{n}_2 \rangle - \langle \hat{n}_1 \rangle = \langle \hat{a}_2^\dagger \hat{a}_2 \rangle - \langle \hat{a}_1^\dagger \hat{a}_1 \rangle. \quad (2.2.4)$$

By making the homodyne detection balanced, the classical noise from each detector thus cancels out (as the classical noise from each detector is the same), leaving us

¹²Furthermore, it turns out that it is a necessary condition for the transformation to be unitary.

only with the quantity of interest; the quantum noise. From equation (2.2.3) it is seen that

$$I_- = \sqrt{2}|\alpha_{LO}|\hat{q}_\theta. \quad (2.2.5)$$

Homodyne detection thus enables us to measure the quadrature distribution at an angle defined by the *relative phase difference* of the small signal and the local oscillator. By mounting a mirror on a piezo somewhere along the path of either beam (see Figure 3.1), we can control this phase difference experimentally. In this manner, we can obtain statistics of the quadrature distributions 'all around the clock', or, equivalently, the marginal distributions of the Wigner function at all angles (i.e., we get datasets $\{\theta, q_\theta\}$). From these we proceed to reconstruct the Wigner function by using the maximum likelihood algorithm.

2.2.2 Maximum likelihood algorithm

As described in sections 2.1.4 and 2.1.6, all information about a quantum state is contained in the density operator, or, equivalently, the Wigner function, since there is a one to one relation between the two [7, Section 3.1.2]. As homodyne measurements are state reductive and their outcome therefore is of stochastic nature, we cannot uniquely determine the density operator from any finite number of quadrature measurements. We can, however, perform a large number of measurements, and with some certainty find the most *likely* density operator. If the number is large enough, we can safely assume that we are beyond reasonable doubt.

From a balanced homodyne measurement there are at least two ways to go about the business of reconstructing the quantum state of the light, namely the inverse Radon transformation [7] and the maximum likelihood algorithm (MaxLik). We have chosen to use the latter, since it has several advantages [8] over the former. As the name implies, the MaxLik procedure does indeed do what we desire; given a dataset $\{\theta, q_\theta\}$, it finds the density matrix that maximizes the likelihood of obtaining that specific data. The following presentation is based on [8] and [12, Section 5.2.2].

Basic idea

We start out by presenting the general idea of the algorithm. For a given set of state projective measurement outcomes, $\{x_i\}$, corresponding to apparatus eigenstates $|x_i\rangle$ appearing with relative frequencies f_i , the likelihood of obtaining this data is, denoting the density operator for the state we measure $\hat{\rho}$,

$$\mathcal{L}(\hat{\rho}) = \prod_i \text{pr}_i^{f_i} = \prod_i \langle x_i | \hat{\rho} | x_i \rangle^{f_i} = \prod_i \text{Tr} \left(\hat{\Pi}_i \hat{\rho} \right)^{f_i}, \quad (2.2.6)$$

where obviously pr_i is the probability of outcome x_i , and $\hat{\Pi}_i$ is the projection operator $\hat{\Pi}_i = |x_i\rangle\langle x_i|$. It is clear that for the density operator that maximizes the likelihood, let us denote it $\hat{\rho}_0$, we have that $\text{pr}_i \propto f_i$. Furthermore, we have by completeness of eigenstates of Hermitian operators that $\sum_i \hat{\Pi}_i \propto \hat{1}$ (the identity operator). It therefore follows that if we define the recursion operator $\hat{R}(\hat{\rho})$ by

$$\hat{R}(\hat{\rho}) = \sum_i \frac{f_i}{\text{pr}_i} \hat{\Pi}_i, \quad (2.2.7)$$

then

$$\hat{R}(\hat{\rho}_0) \propto \hat{1}, \quad (2.2.8)$$

implying that

$$\hat{R}(\hat{\rho}_0)\hat{\rho}_0\hat{R}(\hat{\rho}_0) \propto \hat{\rho}_0. \quad (2.2.9)$$

The name of the recursion operator now becomes reasonable as we take equation (2.2.9) as the basis for the actual algorithm. We choose an arbitrary¹³ initial density matrix $\hat{\rho}^{(0)}$ proportional to identity perhaps (but of course with unit trace), and then apply repetitive iterations defined recursively by

$$\hat{\rho}^{(k+1)} = \mathcal{N} \left(\hat{R}(\hat{\rho}^{(k)}) \hat{\rho}^{(k)} \hat{R}(\hat{\rho}^{(k)}) \right). \quad (2.2.10)$$

Where \mathcal{N} is a normalization constant to ensure a trace of unity, such that we have a physically sound density matrix at each step in the algorithm. The operator of equation (2.2.10) will converge monotonically towards $\hat{\rho}_0$, [12, Page 20]. One should be aware that if this should ever be carried out in real life, the Hilbert space in which this scheme takes place must be restricted to having finite dimensionality, such that the operators will be matrices and a computer (equipped with MATLAB, for instance) can do the iteration.

Application to homodyne detection

When applying the algorithm to homodyne detection, it would perhaps seem like a natural choice to work in the basis of quadrature eigenstates $|\theta, q_\theta\rangle$, where

$$\hat{\Pi}(\theta, q_\theta) = |\theta, q_\theta\rangle \langle \theta, q_\theta|. \quad (2.2.11)$$

However, working in a basis of quadrature eigenstates is no easy task, and we therefore want to change basis to the Fock states, in which the density operator is actually a matrix¹⁴. The projection operator is then

$$\hat{\Pi}_{mn}(\theta, q_\theta) = \langle m | \theta, q_\theta \rangle \langle \theta, q_\theta | n \rangle. \quad (2.2.12)$$

This overlap is just the stationary solution to the Schrödinger equation describing a particle moving in a harmonic potential, given by [12, Equation 2.72] as

$$\begin{aligned} \langle n | \theta, q_\theta \rangle &= e^{in\theta} \langle n | 0, q \rangle \\ &= e^{in\theta} \frac{1}{\sqrt{\pi}} \frac{H_n(q\theta)}{\sqrt{2^n n!}} e^{-q_\theta^2/2}, \end{aligned} \quad (2.2.13)$$

where H_n is the Hermite polynomial of n^{th} order. Although we changed basis to a countable one, we are still in a position of having continuous data from the detection. The solution to this problem is to bin the data according to values of θ and the measured quadrature value. Of course, precision will be lost as long as the bin size is finite, but with small enough bins, such that¹⁵ f_{θ, q_θ} is either 0 or 1, we should be alright [8]. As a final correction before starting up the computer, we are forced to make a cut-off of the dimension of the Hilbert space. That this is of no great concern to us, is evident when working in the Fock basis and considering squeezed vacuum (recall Figure 2.2). Of the infinity of Fock states, one should never expect to find more than, say, 11 photons in the vacuum.

¹³Please note that the result of our algorithm should ideally be completely independent of our choice of initial operator, whereas the number of iterations before convergence obviously depends on it. Luckily, this turned out to be the case, see Table 3.3.

¹⁴Since the set of eigenstates is countable.

¹⁵Now f denotes an absolute frequency.

Chapter 3

The experiment

With the quantum optical theory now at hand, we turn our attention towards the main event: the actual experiment. An overview of the experiment is seen in Figure 3.1, where it is also indicated that the experiment may be conveniently described in four main parts, namely

1. The laser
2. The frequency doubling (SHG)
3. The (degenerate) parametric down conversion (OPO)
4. The balanced homodyne detection

These four parts will be described individually in four subsequent sections, providing the theory and practical knowledge needed to undertake the assignment of operating that particular part of the experiment. We shall include actual recorded data in a way so as to support the claims made in the text, and keep a strong focus on the operation of the SHG. But first of all, let us look at the experiment in a more general way.

3.1 Design of the experiment

For the choice of our squeezing apparatus, we follow in the footsteps of the famous work done by Breitenbach et al. [4], and use a two-step mechanism consisting of an

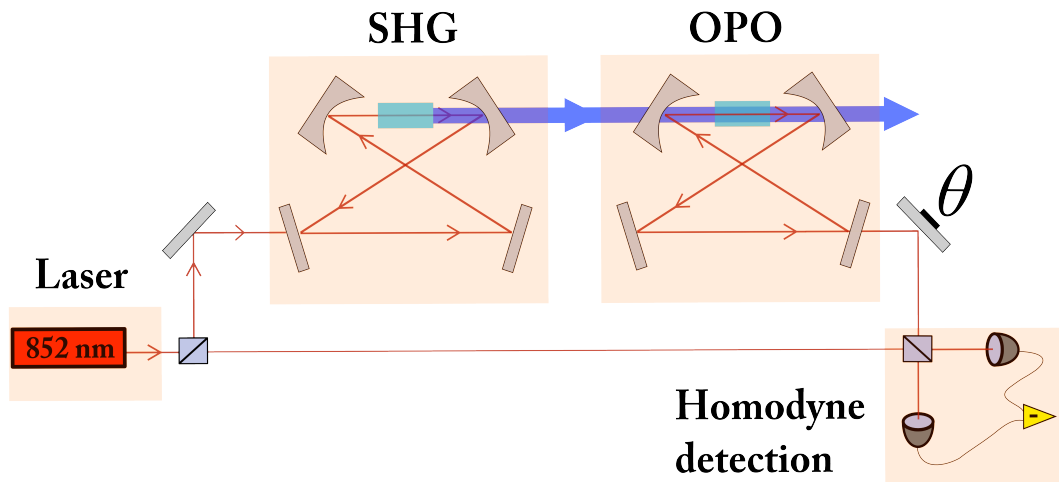


Figure 3.1: Outline of a simplified version of the squeezing apparatus.

SHG followed by an OPO. This is a smart setup for various reasons.

At the end of the day, we want to detect squeezed light, but not just at any old wavelength. Rather, we want the light to be on resonance with the D2 line in cesium, i.e. the squeezed light should have a wavelength of 852nm¹⁶. Since the actual squeezing takes place in the OPO (see Section 3.4) by the conversion of one photon into two, corresponding to a halving of frequency, we get squeezed light at twice the wavelength of the pumping light. At first sight, one would then perhaps suggest using a 426nm laser as the pump for the OPO, but this idea was refused for (at least) two reasons. First of all, you would need to have two working lasers, one operating at 426nm and the other at 852nm, in order to perform the homodyne detection whereas our scheme only requires one. Apart from that, it is of utmost importance for the homodyne detection, that the local oscillator is phase coherent with the signal field. By first using an SHG for frequency doubling and afterwards an OPO for squeezing and frequency halving, you can make do with the same single master laser, and thus get the phase coherence for free.

3.2 Laser and the laser light

The laser light used comes from a Titanium Sapphire laser (Ti:Sa) tunable in the range from about 850 nm to 860 nm. The laser is optically pumped by a Verdi V10 laser. The Ti:Sa laser is operated in such a way that it provides a continuous and single mode signal [1, Section 6.1]. The output power provided by the laser is up to 600mW, and when the squeezing experiment is running, we are using most of it. For a more detailed description of the laser set up see [11, Section 4.1].

When working on an optical table, it is crucial to know how laser light behaves. If one desires to send the light into a cavity, transmit it through an optical fiber or mix two beams, the spatial profile of the light must be taken into consideration. One often speaks of *coupling into* (e.g.) a cavity. The meaning hereof is qualitatively understood as "getting the light to not just bounce off the mirrors, but actually stay within the cavity for several roundtrips and interfere with itself" or, equivalently, "making the light fit into the cavity". The key word here is interference; if we are to observe proper interference phenomena, the light has to be almost perfectly overlapped. In order to overlap two things, their shapes must be known.

3.2.1 Incoupling 1: The Gaussian beam

In this section and the next, we give a presentation of how one can successfully picture the shape of light, and use this knowledge to obtain the desired incoupling. We base the following on [17, Chapters 2 and 3] and [9, Chapter 14], respectively.

As should be apparent to anyone who has ever seen a laser beam, there must be more to the story of light as electromagnetic waves than just the two well-known solutions to the wave equation, plane and spherical waves,

$$\mathbf{E}(\mathbf{r}, t) = \mathcal{E}(\mathbf{r}, t)e^{-i(\mathbf{k}\cdot\mathbf{r}-\omega t)}\mathbf{k} \quad (\text{plane waves}), \quad (3.2.1)$$

$$\mathbf{E}(\mathbf{r}, t) = \frac{\mathcal{E}_0(t)}{r}e^{-i(kr-\omega t)}\hat{\mathbf{r}}. \quad (\text{spherical waves}), \quad (3.2.2)$$

since neither of these possess both of the essential features of a laser beam, namely unidirectionality and transverse locality. The plane waves are extremely unidirectional, but unfortunately extend to infinity in both directions perpendicular to the

¹⁶This specific choice of wavelength has nothing to do with the squeezing as such, but stems from some of the long term projects of Quantop, as described in the introduction.

wave vector. There is thus not much hope of ever focusing any finite amount of power into any optical element of finite dimensions using plane waves! The spherical waves, on the other hand, are somewhat confined in space, since their amplitude decreases as r increases, but these waves travel in all directions away from the light sources. This would obviously put some very unpractical constraints on our optical tables. It is clear that we must find a new waveform to describe the light beam coming from a laser. The requested waveform will be found as the Gaussian beam. A more detailed derivation of the results simply stated here can be found in Appendix C.

Starting out with a monochromatic wave

$$E(\mathbf{r}, t) = \mathcal{E}(\mathbf{r})e^{-i\omega t}, \quad (3.2.3)$$

and the assumption that

$$\mathcal{E}(\mathbf{r}) = \mathcal{E}_0(\mathbf{r})e^{ikz}, \quad (3.2.4)$$

it can be shown that taking

$$\mathcal{E}_0(\mathbf{r}) = \frac{C}{q(z)} \exp \left[ik \frac{\rho^2}{2q(z)} \right], \quad q(z) = z + iz_0, \quad \rho^2 = x^2 + y^2, \quad (3.2.5)$$

yields the Gaussian beam, which has the desired properties of unidirectionality and spatial confinement. The function $q(z)$ is called the q -parameter (a very essential parameter, as explained in the next section) and z_0 is known as the Rayleigh range. The inverse of the q -parameter can be divided into a real and imaginary part in the following way:

$$\frac{1}{q(z)} = \frac{1}{R(z)} + \frac{i\lambda}{\pi w(z)^2}, \quad (3.2.6)$$

where $w(z)$ and $R(z)$ are real. Here $w(z)$ is called the spotsize¹⁷ (this can be interpreted as the radius of the beam), and $R(z)$ is called the radius of curvature. We note that the beam will be slimmest at $z = 0$, which gives rise to the notion of the beam having its *waist* at this location. By comparing equations (3.2.5) and (3.2.6), one obtains the expressions

$$R(z) = z + \frac{z_0^2}{z} \quad (3.2.7)$$

$$w(z) = w_0 \sqrt{1 + \frac{z^2}{z_0^2}}, \quad \text{where} \quad w_0 = \sqrt{\frac{\lambda z_0}{\pi}}. \quad (3.2.8)$$

The name 'Gaussian beam' stems from the beam's intensity distribution (in a plane transverse to the propagation direction). This quantity is proportional to the field squared, and therefore given by

$$I = I_0 \frac{w_0^2}{w(z)^2} \exp \left[\frac{-2\rho^2}{w(z)^2} \right]. \quad (3.2.9)$$

Measuring this intensity will be of great importance to us in the laboratory, when we want to determine the value of q , as will be described in Section 3.2.3.

¹⁷The cross-section of the beam is still infinite in principle, but rapidly decreasing, as we shall see.

3.2.2 Incoupling 2: Propagation through optical elements

As was mentioned above, the q -parameter is the quantity we are really interested in when it comes to incoupling. This is due to the fact that the propagation of a Gaussian beam through different optical elements is easily described via the so-called $ABCD$ -law for Gaussian beams. It is shown in [9, Section 14.6] that using the classical ray matrices for optical elements,

$$\mathbf{M}_{Lens} = \begin{bmatrix} 1 & 0 \\ -1/f & 1 \end{bmatrix} \quad (\text{for a lens of focal length } f), \quad (3.2.10)$$

$$\mathbf{M}_{Free} = \begin{bmatrix} 1 & d \\ 0 & 1 \end{bmatrix} \quad (\text{free propagation the distance } d), \quad (3.2.11)$$

$$\mathbf{M}_{Curved} = \begin{bmatrix} 1 & 0 \\ -2/R & 1 \end{bmatrix} \quad (\text{for a curved mirror w. ROC}^{18}R), \quad (3.2.12)$$

and describing the total effect of propagation through a system of optical elements as the matrix product of optical matrices¹⁹

$$\mathbf{M} = \begin{bmatrix} A & B \\ C & D \end{bmatrix}, \quad (3.2.13)$$

the q -parameter of the Gaussian beam will obey the $ABCD$ -law:

$$q_f = \frac{Aq_i + B}{Cq_i + D}, \quad (3.2.14)$$

where q_i is the initial q -value and q_f is the final value, after propagation through the system described by \mathbf{M} . This law is very fundamental and of frequent use in any optical laboratory where lasers, mirrors and lenses are being used.

We can now finally give a quantitative criterion for coupling into a cavity. As a cavity consist of mirrors, the effect of one roundtrip in the cavity will be described by some optical matrix

$$\mathbf{M}_{Cav} = \begin{bmatrix} a & b \\ c & d \end{bmatrix}. \quad (3.2.15)$$

For the incoming beam to be a stable mode of the cavity, the beam must be prepared in such a way that its q -value just as it enters the cavity fulfils the demand that

$$q = q_i = q_f \quad \text{or equivalently that} \quad q = \frac{aq + b}{cq + d}. \quad (3.2.16)$$

The scheme for incoupling is therefore to first set up the cavity²⁰, calculate the resulting optical matrix, determine the required value of q , and then manipulate the laser beam with mirrors and lenses, so that the stability criterion is met. Appantly, measuring q is now an important experimental task.

3.2.3 Measuring the q parameter

From equations (3.2.6), (3.2.7) and (3.2.8), we see that our laser beam is fully determined for all values of z as soon as we know the width of the beam waist (w_0) and where it is (where to set $z = 0$). All this information is contained in the spotsize

¹⁸ROC = Radius Of Curvature.

¹⁹With the optical matrix of the first element furthest to the right in the matrix product, etc.

²⁰In any arbitrary way? -No, see section 3.3.

function of equation (3.2.8), making $w(z)$ the only function we need to determine by measurement.

Basically, we followed three different approaches in the measurement of $w(z)$, as described below. They all make use of the Gaussian intensity distribution of the light.

Intensity profile

As seen from equation (3.2.9), the intensity distribution in a plane perpendicular to the direction of propagation of the beam (i.e. the xy -plane) will be a rotational symmetric Gaussian distribution. Approximately 68% of the intensity will then be confined within a circle of radius $w(z)$. Thus, determining $w(z)$ amounts to determining the width (more precisely: the half width at half maximum (HWHM)) of the intensity profile. Doing this at different distances, z_i , from the source, will then yield datapairs of the type $(z_i, w(z_i))$ enabling us to determine $w(z)$ by fitting equation (3.2.8) to our data.

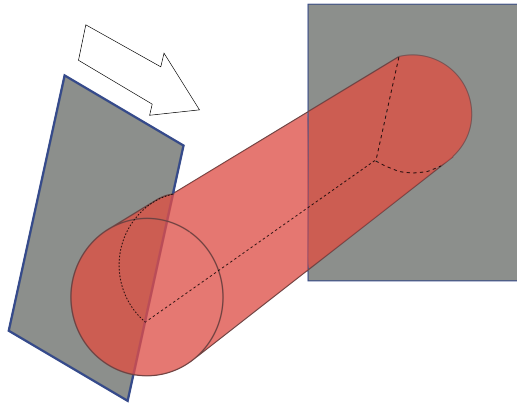


Figure 3.2: The razorblade blocks the laser beam.

The razorblade method

The idea behind the razorblade method is placing a photodetector in a position where it detects more or less all of the beam's intensity (well beyond 99%), and then slowly blocking more and more of the beam, until the intensity is reduced by 16%. Going even further with this, one eventually blocks half of the light intensity. According to our assumption, the distance (in the, say, x -direction) between the 16%- and 50%-blocking of the beam is then the HWHM. Obviously, the method has its name from the razorblade one uses to do the blocking. See Figure 3.2.

In practice, however, instead of a razorblade we used a Unibrain Fire-i camera with a 680×480 pixels resolution and a linear intensity response ranging from 0 to 255 units pr. pixel. Taking a snapshot of the laserbeam then gave a 83558400 cubed units 3D-picture of the intensity profile. Converting this into a matrix and using simple linear algebra, we could find the row or column (counting from the center) at which the intensity had been reduced by a factor of 0.16. Knowing the pixel size, this gave us the desired number. By measuring in two orthogonal directions, interference phenomena such as fringes in the intensity profile became less significant. See Figure 3.3(a) for a camera snapshot of the beam.

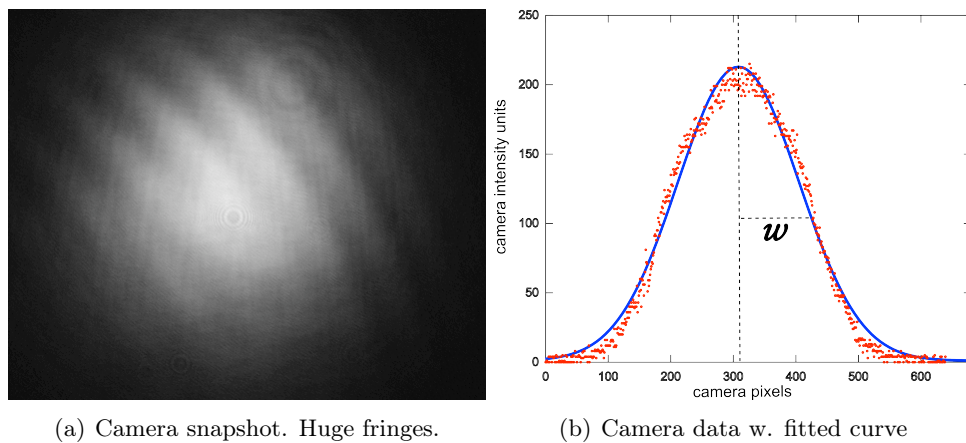


Figure 3.3: Data from the camera. The fitted data is not from the snapshot shown, but a different, more well-behaved one.

Just fitting

But since these snapshot-matrices were at our disposal, we felt inclined towards simply fitting a Gaussian function to the row or column at the center of the beam picture. With at least 480 datapoints to fit against, the width should be rather well-defined. The center row or column would of course still have to be identified using the razorblade method, but if nothing else, these Gaussian fits would provide a good indication of whether our camera did in fact have a linear response or not. A fit made to a Gaussian using such a center row is seen in Figure 3.3(b). It seems like a trustworthy camera, after all.

3.2.4 Japanese Swinging Stick

As it turned out, different practical difficulties arose in connection with the use of the camera, and averaging did not remove the discouraging interference effects. A somewhat singular way to perform the desired measurement was introduced as the 'japanese swinging stick method'. The method takes as its foundation not so much the Gaussian intensity distribution as its *integrated* intensity distribution, the Error Function (see Appendix A). The actual measurement then amounts to letting a stick of width much (a few times) larger than the beam swing in front of the beam and having a photodetector record the intensity over time. This picture (intensity as a function of time) is then fitted against an Error Function, and the spotsize is obtained, see Figure A.1.

Note that the speed at which the stick swings through the beam is (from conservation of energy) dependent on the height from which the center of mass of the stick starts out, i.e. the initial angle of the stick. We have made no reference hereto in our outline of this particular method of obtaining the spotsize, and it should be stressed that only an approximate value can be expected. The true power of this method lies in its speed, not its accuracy²¹.

As the incoupling now has been taken care of, we are able to put a crystal inside our cavity and experience second harmonic generation. There is a bit more to the story on how to actually achieve this, as will be explained in the next section.

²¹However, speed and accuracy are linked together through statistics. One should prefer this method unless extreme precision is required.

3.3 SHG

In this section, we shall explain how to operate the second harmonic generator. The section is divided into two parts, where we first present the necessary optimization of both crystal and laser beam, and then proceed to characterize our particular SHG.

3.3.1 Outline

The process of second harmonic generation, also referred to as frequency doubling, is a nonlinear optical process, in which an incoming light beam at a frequency ω , which we shall call the fundamental wave, generates an output beam at the frequency 2ω , the second harmonic wave. In order to obtain the highest possible input power for the OPO, we shall need a high conversion efficiency for the frequency doubler. To optimize this, we shall consider the situation of a laser beam going straight through a crystal. We apply a classical (Lorentz) model of the atom-light interaction, following [9], to find the conversion efficiency, η . The derivation is carried out in Appendix B. One arrives at the following intensity for the frequency doubled field after it has passed through a crystal of length ℓ

$$I_{2\omega}(\ell) = 2 \left(\frac{\mu_0}{\epsilon_0} \right)^{3/2} \frac{\omega^2 \bar{d}^2}{n^2(\omega)n(2\omega)} I_\omega(0)^2 \ell^2 \left(\frac{\sin(\frac{1}{2}\Delta k \ell)}{\frac{1}{2}\Delta k \ell} \right), \quad (3.3.1)$$

where ϵ_0 and μ_0 are the usual vacuum permittivity and permeability, respectively, n is the index of refraction and \bar{d} is explained in Appendix B. The conversion efficiency will then be given as

$$\eta = \frac{I_{2\omega}(\ell)}{I_\omega(0)} = 2 \left(\frac{\mu_0}{\epsilon_0} \right)^{3/2} \frac{\omega^2 \bar{d}^2}{n^2(\omega)n(2\omega)} I_\omega(0) \ell^2 \left(\frac{\sin(\frac{1}{2}\Delta k \ell)}{\frac{1}{2}\Delta k \ell} \right)^2. \quad (3.3.2)$$

From this, it is evident that the conversion efficiency is highly dependent on the phase mismatch $\Delta k = k_{2\omega} - 2k_\omega$, and has a maximum for $\Delta k = 0$. The process of optimizing this parameter for maximum intensity is called phase matching. However, the phase matching condition is not the end of the story. A more detailed theory is needed, and will be described in Section 3.3.3.

3.3.2 Phase matching

The physical situation is easy to grasp: As the fundamental and the second harmonic wave propagate through the nonlinear medium, they will interfere with each other. In some regions of the crystal the interference will be destructive, in other regions constructive. We have so far said nothing about the direction of the second harmonic beam, but we now see that only some directions are possible in order for the second harmonic wave not to get killed by inference. Since the two waves travel with different phase velocities in the crystal, the allowed regions must somehow be determined by the phase mismatch, and this is exactly what is qualitatively contained in the factor $\sin^2(\frac{1}{2}\Delta k \ell)/(\frac{1}{2}\Delta k \ell)^2$ in equation (3.3.2) [9, Section 17.6].

A totally different way of viewing this is using a picture of photons [17, Chapter 21] being created and annihilated within the crystal. Every time we get a photon of the frequency doubled light out, conservation of energy demands that two photons of the fundamental light must have vanished, since $2\omega_f = \omega_{SHG}$. Similarly, conservation of momentum requires that the wave numbers obey the relation $2k_\omega = k_{2\omega}$, which is equivalent to demanding $\Delta k = 0$.

In practice, the phasematching condition can be met in two different ways, by either turning the crystal (angle phase matching) or controlling its temperature (temperature phase matching). Instead of doing actual phasematching, one can also use the so-called *quasi*-phasematching.

Angle and temperature phase matching

In the scheme of angle phase matching we shall need a uniaxial birefringent crystal. In such a crystal [9, Chapter 17], only waves with polarization perpendicular (ordinary waves) or parallel (extraordinary waves) to the plane spanned by the direction of propagation and the optic axis can propagate. The key point is now that whereas the refractive index of the ordinary wave, n_o , remains fixed, the refractive index of the extraordinary wave, n_e , depends on the angle θ . Letting the fundamental wave be the extraordinary wave and the second harmonic be the ordinary wave, it is shown in [9, Section 17.6] that phase matching is obtained whenever

$$\frac{1}{n_o^2(2\omega)} = \frac{1}{n_e^2(\omega, \theta)} = \frac{\cos^2 \theta}{n_o^2(\omega)} + \frac{\sin^2 \theta}{n_e^2(\omega)}. \quad (3.3.3)$$

The situation is shown in Figure 3.4, from which it is also clear that θ is easily controlled in the laboratory; one simply turns the crystal²².

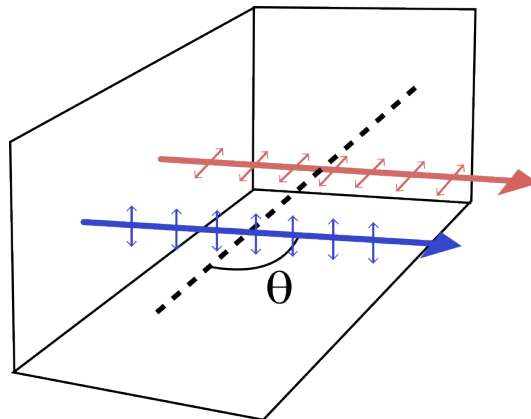


Figure 3.4: Propagation through a crystal. The dashed line indicates the optic axis. The (infra) red and the blue light have orthogonal polarizations.

The basic problem of getting two waves with different phase velocities to interfere constructively can also be solved by exploiting the fact that different light waves of different wavelengths experience different temperature dependencies of the refractive index (in certain crystals) [9], as is the case with the angular dependence in angle phase matching. By keeping the temperature fixed at the right value, phase matching can thus be achieved. Since temperature fluctuations are always present in a realistic experimental situation, this on the other hand calls for a temperature control system, regardless of whether we use angle phase matching or not.

Quasi phase matching

There is no such thing as a free lunch, and this is especially true in experimental physics, where everything is a trade-off. Often the choice of crystal that provides

²²In real life one usually buys a crystal already cut in an angle tailored for the wavelengths in question.

you with ideal phase matching, has additional discouraging features, such as a low non-linear coefficient²³ or other disadvantages. It is therefore sometimes, and indeed in our actual experimental setup, better to allow a phase mismatch, and then compensate by other means. In particular, what we used was a PPKTP²⁴ crystal with a periodic structure that reverses the sign of the mismatch. Viewing the factor $\frac{1}{2}\Delta k\ell$ in equation (3.3.2) as the accumulated phase mismatch along the entire length of the crystal, we see how quasi phase matching works; with Δk constantly changing sign (equally much to each side), no great phase mismatch ever accumulates, and thus the efficiency remains high.

Our treatment of optimizing second harmonic generation has so far only dealt with the problem of getting the crystal to behave. In the next section, we shall discuss how to optimize the incoming laser.

3.3.3 Optimal waist

According to Boyd and Kleinmann in [3], the output power of the frequency doubler can be significantly increased by considering other aspects than those contained within the framework of the Lorentz model. In the following we shall consider, primarily, where, and how large, the laser waist should be with respect to the given crystal. In the crystal, the dependence of the converted power upon optimizable parameters can be expressed through the following 'h-function'

$$h(\sigma, \beta, \kappa, \xi, \mu) = \left(\frac{\pi^2}{\xi}\right) e^{\mu a \ell} F(\sigma, \beta, \kappa, \xi, \mu), \quad (3.3.4)$$

where

$$F(\sigma, \beta, \kappa, \xi, \mu) = \left(\frac{2}{\sqrt{\pi}}\right) \int_{-\infty}^{\infty} ds |H(\sigma + 4\beta s, \kappa, \xi, \mu)|^2 e^{-4s^2} \quad (3.3.5)$$

and

$$H(\sigma', \kappa, \xi, \mu) = (2\pi)^{-1} \int_{-\xi(1-\mu)}^{\xi(1+\mu)} \frac{d\tau'}{1 + i\tau'} e^{-\kappa\tau'} e^{i\sigma'\tau'}. \quad (3.3.6)$$

The different variables are explained in Table 3.1.

we shall neglect the absorption and choose the middle of the crystal as focus. This is shown to be the optimal place of focus in [3], where it is also shown that the absorption inside the crystal has almost the same effect as regular linear losses. This allows us to set $\kappa = \mu = 0$.

If the dimensions of the crystal are fixed, one obtains

$$h(\sigma, B, \xi) = h(\sigma, B\sqrt{\xi}, 0, \xi, 0), \quad (3.3.7)$$

where $B = \frac{1}{2}\rho\sqrt{l \cdot k_\omega}$, and k_ω is the wavenumber of the fundamental beam in the crystal. The heavy theory thus all boils down to maximizing a function of two variables. The function is shown in Figure 3.5. The optimal parameters turns out to be

$$\xi_{max} = 2.84 \quad (3.3.8)$$

$$\sigma_{max} = 0.574. \quad (3.3.9)$$

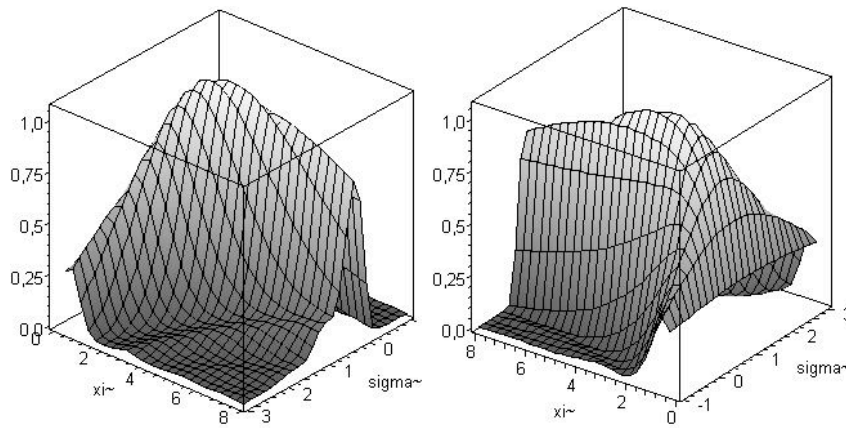
Using the dimensions of the crystal, one then finds the optimal waist. For the crystal used in our setup the dimension where $20 \times 1 \times \text{mm}$, yielding a value of $w_{opt} = 31.7 \mu\text{m}$ for the width of the optimal waist.

²³The material dependent coefficient a mentioned in Appendix B.

²⁴Periodic Poled Potassium Titanyl Phosphate.

σ	$\sigma = \frac{1}{2}b\Delta k$
κ	$\kappa = \frac{1}{2}\alpha b$
α	$\alpha = \alpha_1 - \frac{1}{2}\alpha_2$
β	$\beta = \frac{\rho}{\delta_0}$
δ_0	$\delta_0 = 2\frac{W_0}{b}$
σ'	$\sigma' = \sigma + 4\beta s$
μ	$\mu = \frac{l-2f}{l}$
ξ	$\xi = \frac{l}{b}$, is also called the focusing parameter
f	The beam focus, i.e. the beam is focused at $z = f$ where $z = 0$ is the beginning of the crystal and z -axis is the direction of propagation of the laser beam
w_0	The waist of the laser beam
ρ	The angle of the doubly refracted extraordinary waves
α_1	The linear losses in the crystal of the fundamental wave
α_2	The linear losses in the crystal of the second harmonic
l	The crystal length
b	The confocal parameter, which is twice the Rayleigh range
Δk	The phase mismatch

Table 3.1: A list of the different variables used in the 'h-function'

Figure 3.5: The unsuperseded h -function from 1968.

3.3.4 Cavity

Having optimized both the crystal and the laser focus, we only need one thing: power! The high intensities needed for second harmonic generation are most easily achieved by placing the crystal inside at cavity, and thus let a strong light field build up. In the following we shall describe the intracavity field considering the setup used in Figure 3.6. The intracavity power builds up according to the relation [1, Section 5.3]

$$\frac{P_{Cav}}{P_{In}} = \frac{T}{(1 - g(\nu))^2}, \quad (3.3.10)$$

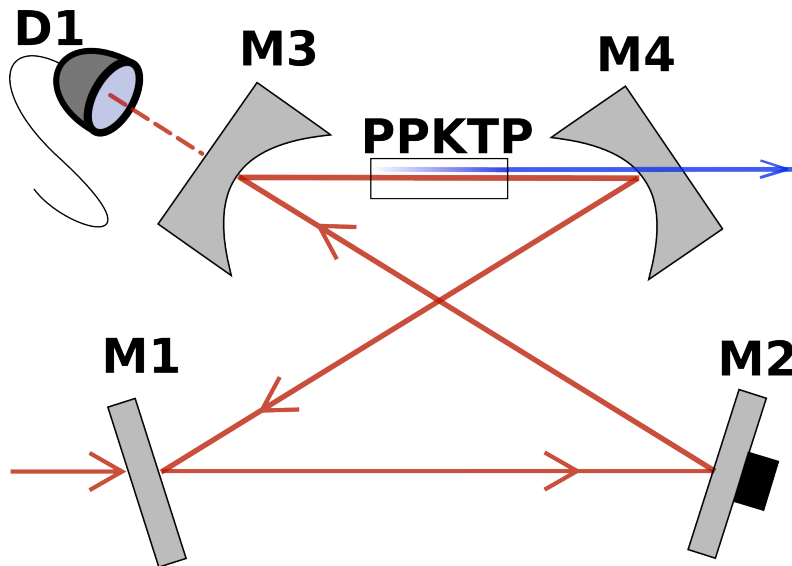


Figure 3.6: The cavity set up used for SHG.

where $g(\nu)$ is the attenuation factor (the factor that the cavity field amplitude is multiplied by after one roundtrip) and T is the transmission coefficient of the incoupler (M1). Considering our cavity setup, we see that²⁵

$$g(\nu) = \sqrt{1 - T} \sqrt{1 - \mathcal{L}} \sqrt{1 - E_{NL} P_{Cav}}. \quad (3.3.11)$$

Here \mathcal{L} is the linear losses, excluding the incoupler, M1, and E_{NL} is the single pass conversion efficiency of the crystal. The conversion efficiency for the cavity is then found to be

$$\eta = \frac{P_{Cav}}{P_{In}} = \frac{T}{(1 - \sqrt{1 - T} \sqrt{1 - \mathcal{L}} \sqrt{1 - E_{NL} P_{Cav}})^2}. \quad (3.3.12)$$

This is a transcendental equation that can be solved numerically.

It is now clear that we shall need to estimate the cavity losses in order to describe the cavity. The losses in a cavity are frequently described by the finesse, see [1, Section 5.3],

$$\mathcal{F} = \frac{\pi \sqrt{|g(\nu)|}}{1 - |g(\nu)|}, \quad (3.3.13)$$

a quantity that can be measured in various way, as will be mentioned in Section 3.3.5. The finesse has a very intuitive interpretation as the average number of roundtrips a photon performs inside the cavity before it is transmitted out of the cavity or absorbed by some loss mechanism [17].

In the next section we present some measurements enabling us to characterize the crystal, cavity and ultimately the performance of the second harmonic generator used in our experiment.

3.3.5 Characterizing the SHG

Once the crystal has been put inside the cavity, and all the optimizing conditions have been met, we are in principle done, and blue light can be detected. We can thus begin to characterize our apparatus. The results are presented in the following.

²⁵The phase shift after one roundtrip is of course $2n\pi$ w. n being an integer in order for us to have continuous constructive interference.

Crystal

The crystal parameter we are interested in is the single pass conversion efficiency, E_{NL} , defined as $E_{NL} = P_{2\omega}/P_{\omega}^2$. This parameter was determined experimentally by removing the outcoupler mirror, M4, and measuring the intensity of the frequency doubled light for different input intensities. In this way, the beam geometry was left unchanged, such that we kept the desired waist found in Section 3.3.3 inside the crystal. The infrared light which is bound to be transmitted by the crystal was simply removed using a filter. Plotting $P_{2\omega}$ as a function of P_{ω}^2 will then give an affine relation with E_{NL} as the slope, see Figure 3.7. The single pass conversion efficiency is found by fitting to be 5.3 \% W^{-1} . This result is way larger than the expected $2\% \text{ W}^{-1}$ (see for example [11, Section 4.2.1]). Initially, we believed that the filter used did not filter out all the infrared light, which would lead to the measured value of $P_{2\omega}$ being too high, thus yielding an unrealistically high E_{NL} . However, upon measuring the transmission of the filter for $\lambda = 852 \text{ nm}$ and finding it to be $T \approx 0.001$, this explanation was abandoned, as we can safely say that we are only measuring the converted light. It is therefore a small mystery that we do not obtain a better result, since the measurements are so straightforward. The only explanation we can give is the rather trivial one, that the measurements of either the input or the converted power must simply be wrong.

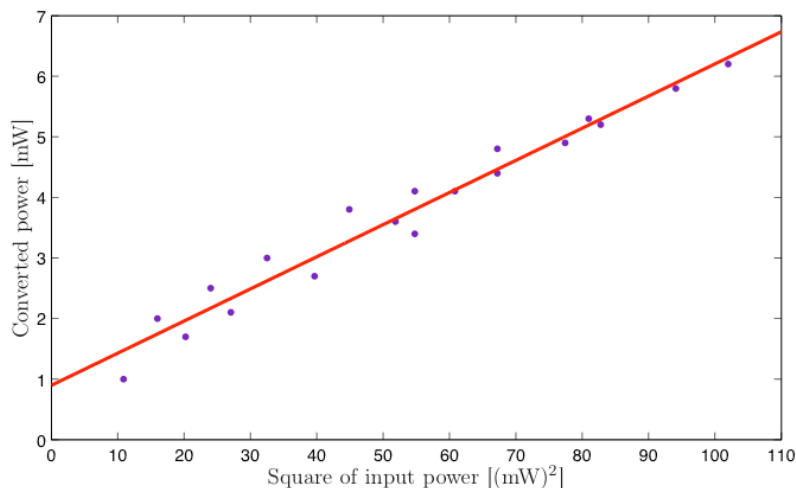


Figure 3.7: Plot of $P_{2\omega}$ as a function of P_{ω}^2 to find the single pass conversion efficiency.

Cavity

The cavity parameter we wanted to investigate was the finesse. If we neglect the losses of infrared light in the crystal, we can find a first guess of the finesse from equation (3.3.13). The mirror properties needed are found in Table 3.2. This yields a finesse in the vicinity of 50.2. Since additional losses are present in the crystal, we shall expect the actual finesse to be lower than this value. Taking the crystal into account, we measure the finesse by fitting Lorentzians [9, Chapter 3] to the transmitted signal (which can be recorded by detector D1 in Figure 3.6), as the cavity's optical pathlength is scanned using the piezo. Using the fact that the finesse fulfills the equation²⁶

$$\mathcal{F} \approx \frac{FSR}{\delta\nu}, \quad (3.3.14)$$

²⁶True when $\mathcal{F} \gg 1$.

where FSR is the free spectral range and $\delta\nu$ is the cavity bandwidth, we then obtain a number for the finesse (see [1, Section 5.3] for an explanation). In doing so, we find the finesse to be 39.7 ± 0.4 .

Mirror	Transmission @ 852 nm
M1	5.7%
M2	low (≈ 0)
M3	0.02%
M4	0.02%

Table 3.2: Mirror properties. M4 has a transmission @ 426 nm of 93.2%. From internal Quantop documentation.

In order to have stable squeezing, we shall need the intensity of blue light to be stable. This is done by applying a Pound-Drever-Hall lock²⁷ [2] to the cavity.

Performance

Finally, we examined the performance of the SHG. The conversion efficiency when the setup is running is depicted in Figure 3.8. We see that a value of approximately 52% can be achieved. This is no world record (see for instance [13]), but indeed enough to feed the OPO.

When the setup is running, we can also test the conversion factor's dependence on the phase matching. The measurements are plotted in Figures 3.8 and 3.9. From our theory, and in particular equation (3.3.2), we would expect to see something proportional to the square of a sinc function. A slight resemblance to this relationship is also seen in Figure 3.9, but both the period and relative size of the peaks are way off. Before dispatching the theory, one should note that due to hysteresis in the crystal and the way the temperature controller works, constantly switching between cooling and heating the crystal thus making it very difficult to actually monotonically increase the temperature, very precise results should not be expected. In the light of this, our results look somewhat convincing, and at least indicate a relationship of *the sort* that we expected.

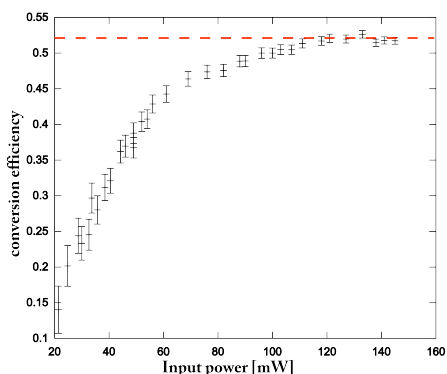


Figure 3.8: Conversion efficiency as a function of the input power. The dashed red line indicates the saturation value.

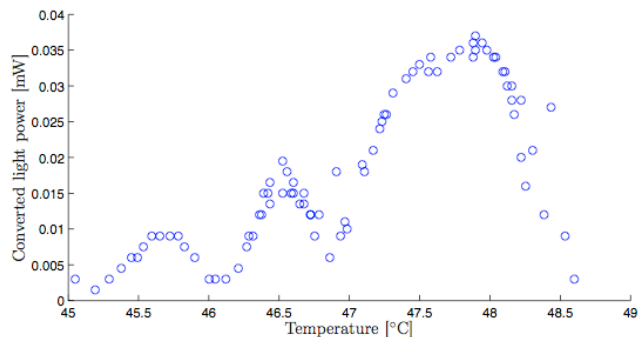


Figure 3.9: Output power as a function of crystal temperature which is proportional to the phasemismatch.

²⁷The locking system itself will not be described here.

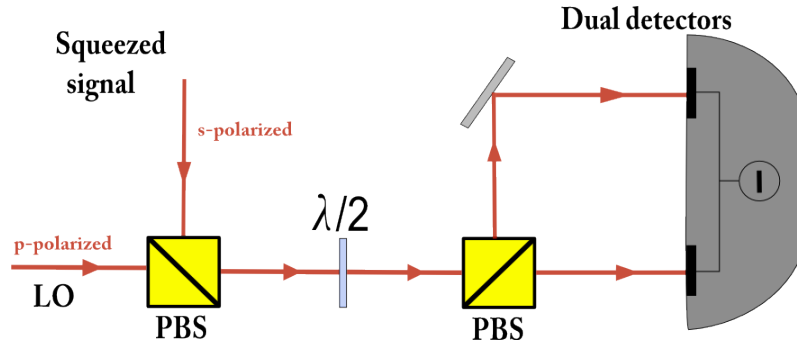


Figure 3.10: The real set up for homodyne detection.

3.4 OPO

We now give a very brief overview of the OPO. We refer the reader to [12] and [11] for additional information.

As it has been described in Section 2.1.7, an OPO is a frequency downconverting mechanism, making it somehow the complementary unit of the SHG. The OPO setup is indeed very similar to that of the frequency doubler, consisting of a running wave cavity and a nonlinear crystal, and just like the SHG it can be locked using a Pound-Drever-Hall locking scheme. It is noted upon inspection of Figure 3.1 that the cavity is resonant for light at 852nm. The blue light that pumps the downconversion is thus transmitted through the cavity and dumped, whereas the infrared (now squeezed) light is frequency filtered by the cavity. In the setup used, the interaction Hamiltonian describing the process is slightly different from the one given in Section 2.1.7. From [10, Section 3.2] it is given as

$$\hat{\mathcal{H}}_I = \frac{i\hbar g}{2} \left(\beta e^{i\varphi} \hat{a}^{\dagger 2} - \beta^* e^{-i\varphi} \hat{a}^2 \right). \quad (3.4.1)$$

Here β is the amplitude of the classical pump field, φ the relative phase associated with the same field, and g the interaction strength. We will not go into an explanation of the differences, but simply remark that taking the time evolution will yield the squeezing operator, with a squeezing parameter $\xi = \beta g \tau$, where τ is the interaction time. We note that both emerging photons are being described by the same field operator, i.e. they are identical. This degeneracy is the reasons for the name *degenerate* optical parametric oscillator. Even though a lot of other photons are produced in and escape from the OPO, we shall only pay attention to the degenerate ones. After the photons emerge from the OPO, they are mixed with the local oscillator field, enabling us to investigate their quantum fluctuations by homodyne detection.

3.5 Homodyne detection

Theoretically speaking, all that is required to perform homodyne detection is a beam splitter and two photodetectors, as already mentioned in Section 2.2.1. In real life, the setup extended to include an extra (polarizing) beam splitter and a half-wave plate. Actual homodyne detection is seen in Figure 3.10.

The beams become spatially mixed in the first PBS, but since they have orthogonal polarization they have not been overlapped. Using a half-wave plate, which rotates the beam's polarizations 45° , the beams will be split 50/50 on the second PBS. After this, the beams are detected, and the homodyne scheme proceeds as explained in Section 2.2.1.

Now, if we are to obtain the maximal amount of information from the detection, we must be sure that the beams are in fact spatially overlapped, i.e., have the same q -parameter (see Section 3.2.1) after the first PBS. This condition is equivalent to having perfect interference between the two beams. We can therefore use the setup as an interferometer, scan the phase, detect fringes and draw conclusions from the overlap. This is a standard procedure, as described in [5, Page 115 and 143].

Detection of the visibility

$$\mathcal{V} = \frac{I_{max} - I_{min}}{I_{max} + I_{min}} \quad (3.5.1)$$

after the second beamsplitter will then yield a measure of the interference. By simple optimization a visibility of $\mathcal{V} = 0.95$ was achieved. This corresponds to an acceptable efficiency.

With the beams successfully overlapped, we shall be concerned with the detector itself, namely it's bandwidth and noise properties²⁸. Since optical frequencies are of the magnitude 10^{14} Hz, there do not exist any detectors able to measure the entire optical spectrum. One therefore sets the zero value of the detector to be at the optical frequency, and then measure around this central frequency. The range on each side in which we can obtain measurements is called the bandwidth of the detector. The detector used had a bandwidth of around 150MHz.

As well as a limit to the frequencies we can measure, there is an upper bound to the powers at which we can detect quantum noise. One speaks of the detector being *shot noise limited* below a certain input power. Shown in Figure 3.11 is the photodetector's response for a range of different input powers. The detector is shot noise limited as long as the response scales linearly with the input. The black line shows a fit against the blue data and has a slope of 0.94. This is a sufficient shot-noise limiting.

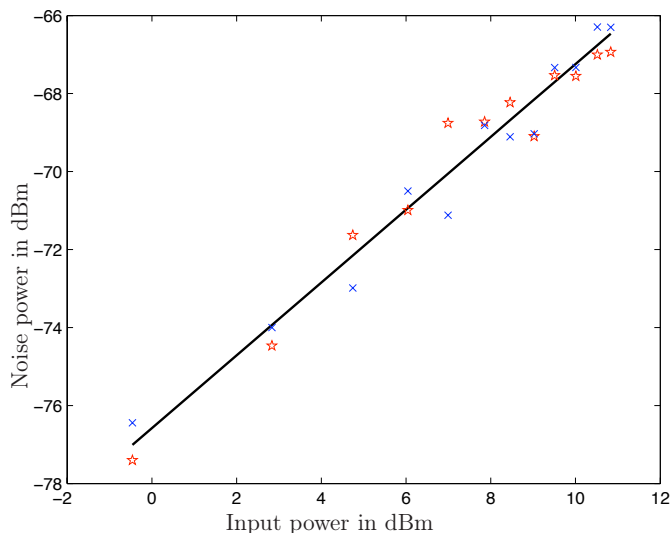


Figure 3.11: Detector noise plotted against the local oscillator's power. Red is for noise at 2Mhz and blue is for 5Mhz.

We have now acquired all the information needed in order to process the data required for quantum tomography.

²⁸As will be mentioned in Section 3.6.3, two sets of photodetectors have produced our data. Both of these have quantum efficiencies above 85%, [11, Section 4.4.1].

3.6 Data presentation

As described in Section 2.2, our final goal is to obtain data relating the angle θ in phase space to at quadrature variance q_θ . However, what we can control experimentally is not θ , but a voltage drop V sent to the piezo. The first thing for us to do is therefore obviously to find the relation between V and θ .

3.6.1 Phase calibration

Shown in Figure 3.12 is the homodyne detection signal's response to the piezo voltage. As the piezo is scanned, the phase changes, but as seen from the figure, the response is not linear, i.e., the period of the sine function is not constant. Rather, we modelled the relation, following [11], as

$$\theta(t) = \omega_1 t^2 + \omega_2 t + \phi. \quad (3.6.1)$$

The connection between V and t is a simple affine function²⁹ that is readily inverted, providing us with $t(V)$. In practice, the time is of course a sample number, scaling linearly with time by the sample rate.

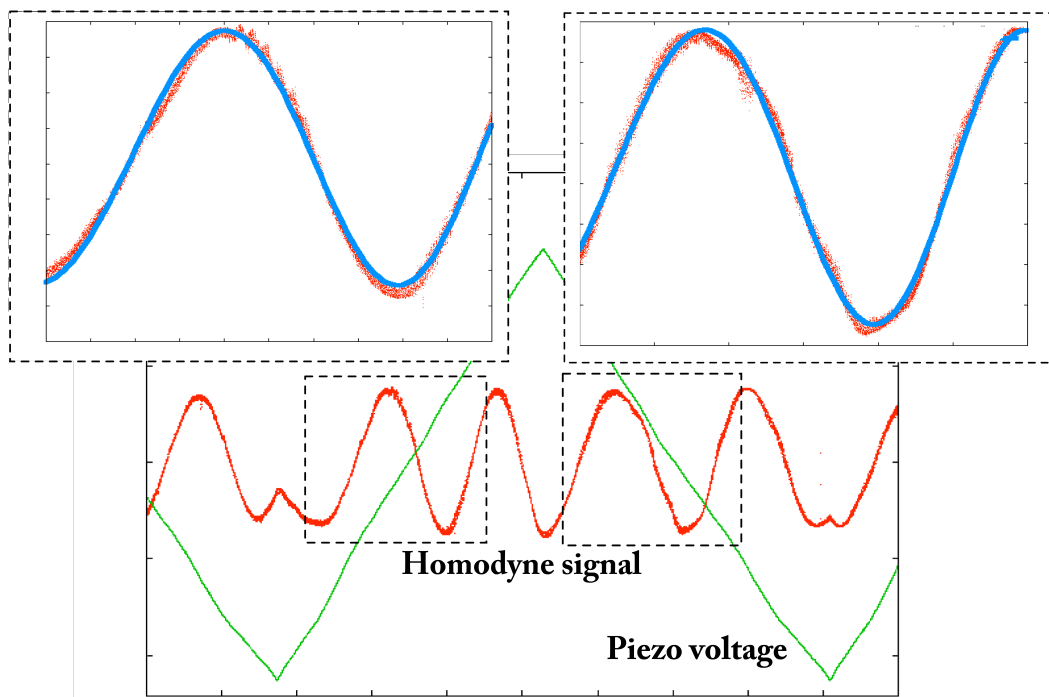


Figure 3.12: Two calibrations, for a rising and a falling piezo voltage, respectively.

We can thus now connect the sample number to the phase θ , and hereby establish the connection between measured quadrature value and phase. The MaxLik algorithm of Section 2.2.2 can finally be fed, and a Wigner function obtained.

3.6.2 Seeing is believing

As a main result we present a figure showing actual squeezing, i.e. a noise reduction below the level set by vacuum. In Figure 3.13 we have depicted the vacuum fluctuations (green) and our squeezed signal (blue). These are the raw signals sent through a spectrum analyser, enabling us to study the frequency component at around 5MHz.

²⁹Scan amplitude times twice the frequency times t plus scan offset.

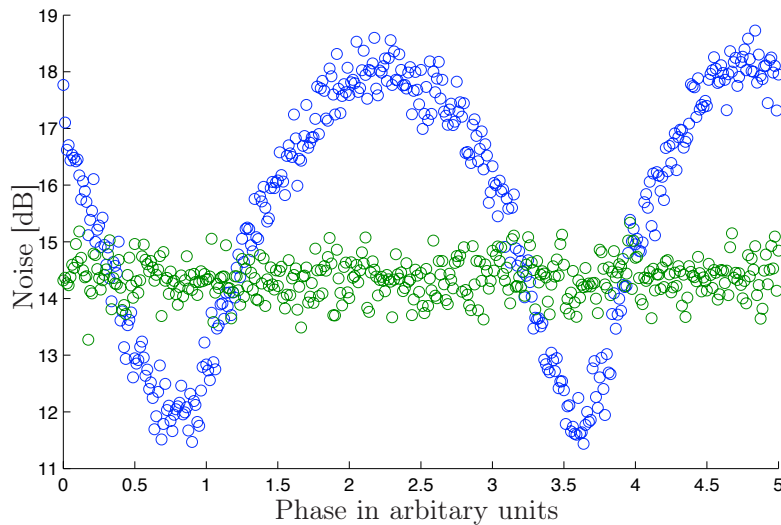


Figure 3.13: As the phase is scanned, the noise @ 1MHZ of the squeezed state changes.

We note that the anti-squeezing is much more outspoken than the squeezing (3.5dB as opposed to 2.2dB). This is a trade-off we are forced to accept, but at least Heisenberg's uncertainty relation has not been broken. This can be considered as a kind of sanity-check of our results.

3.6.3 Reconstructed quantum state

Just seeing squeezing was only the first of our goals. The second, as stated in Section 2.2.2, was to reconstruct the quantum state of the measured light. To achieve this, we implemented the MaxLik algorithm. We urge to remark that the data used for the reconstruction (but not the data of Figure 3.13) was not taken by ourselves, as great obstacles appeared in the laboratory close to our deadline. The data used was given to us by Bo Melholt Nielsen and is produced by the very same equipment that we used, only in 2006 and with a different detector. We now present the results of the reconstruction algorithm.

The reconstructed Wigner function is not as clearly squeezed as the theoretically generated one shown in Figure 2.3(b), but a distinct anti-symmetry is evident from the contour plots in Figure 3.14(b). Furthermore, we see in Figure 3.14(a) that only density matrix elements with both indices being odd³⁰ do not vanish, in accordance with the theoretical prediction of equations (2.1.33) and (2.1.34).

Test of algorithm

However convincing the results of the previous section are, we should not forget that they are the output of a computer algorithm, and not direct measurements. In order to put faith in the results, we must be sure that the reconstruction algorithm works in a trustworthy way. It is difficult to give a quantitative criterion for the trustworthiness of a reconstruction scheme, but in the following we shall present some indications that nothing fishy is going on.

In Section 2.2.2 it is postulated that, working in the Fock basis, the Hilbert space cut-off can be made such that we only include the first 11 states, in other words

³⁰Note that the density matrix shown in the figure is indexed from 1 instead of 0, so that even \rightarrow odd and vice versa.

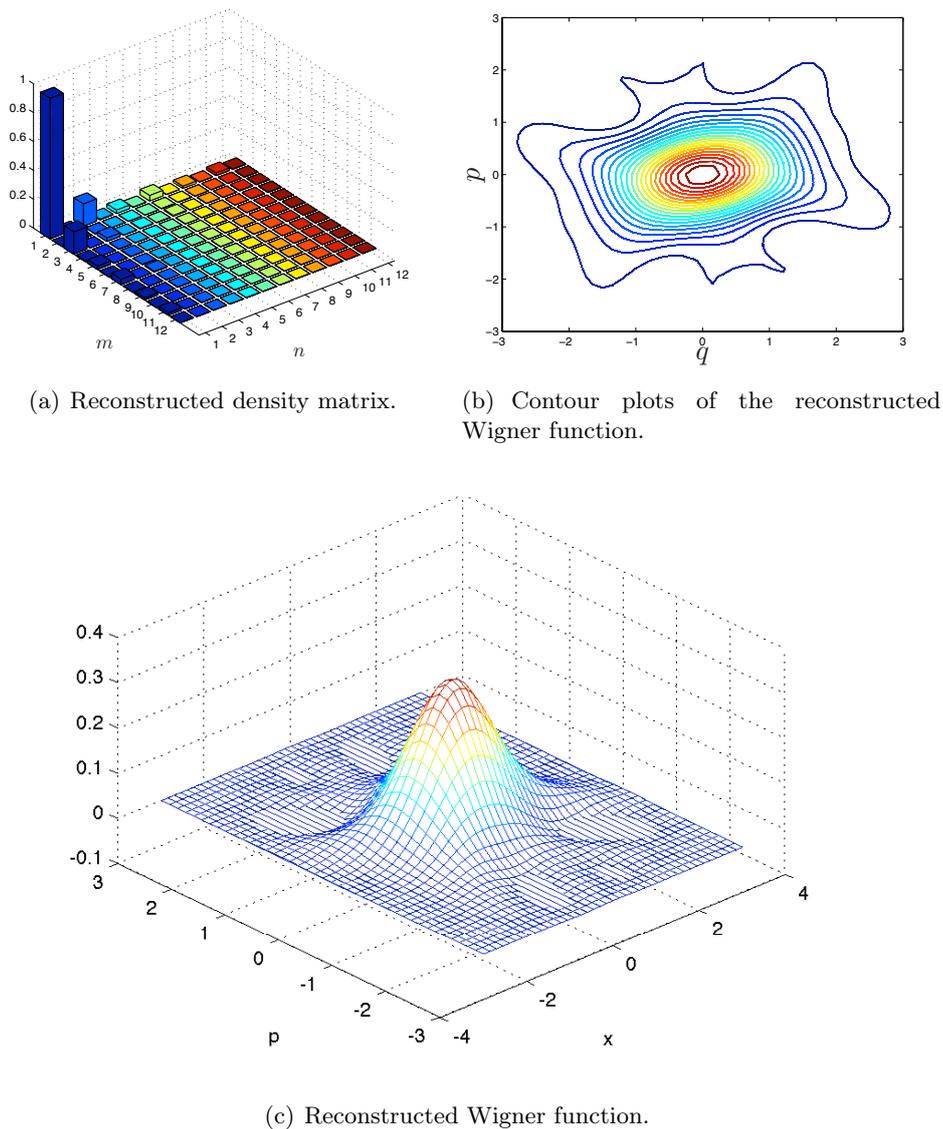


Figure 3.14: The output of the MaxLik algorithm.

$n = 1 \dots N$ where $N = 12$ (again using 1-indexing). We now want to investigate how the reconstruction depends on the choice of cut-off, and whether our initial guess was correct. In Figure 3.15 the contour plots for the reconstructed Wigner function is shown for a range of different cut-off values. Comparing Figures 3.15(a) and 3.15(b) it is seen that taking $N = 12$ changes the shape substantially in comparison with taking $N = 6$. Going even further to $N = 24$, however, does not seem to change things dramatically. Considering the extra amount of computation time needed, around a factor of five for each doubling of N , we conclude that by taking a cutoff for $N = 12$ we obtain enough information in a manageable time.

Another aspect deserving further investigation is the algorithm's dependency of the initial matrix. This dependency better be non-existing, if we are not to be blamed for "guessing" our own results. In Table 3.3 different inputs and outputs are shown. The resulting average photon number is included as a good measure for the similarity of resulting matrices.

The algorithm itself thus seems trustworthy. As a final check, we compare the marginal distributions of the reconstructed Wigner function to the quadrature dis-

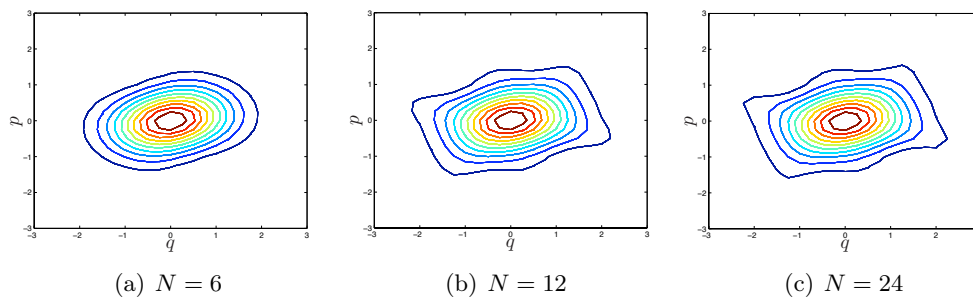


Figure 3.15: Contour plots of the reconstructed Wigner function for different Hilbert space cut-offs.

Initial matrix	No. of iterations	Average photon number
Identity	14	0.065043
Ones	5	0.065043
Random	16	0.065043

Table 3.3: The footnote on page 2.2.2 holds true.

tributions of the raw signal. This is shown in Figure 3.16(b). The plot is made by taking a histogram of around 5000 different measurements made for almost the same phase, (the difference in phase being than 0.02 radians), and comparing it to the related marginal distribution of the constructed Wigner function. We recall from Section 2.1.6 that these two things ideally should be identical, or, for a finite number of measurements, at least resemble one another.

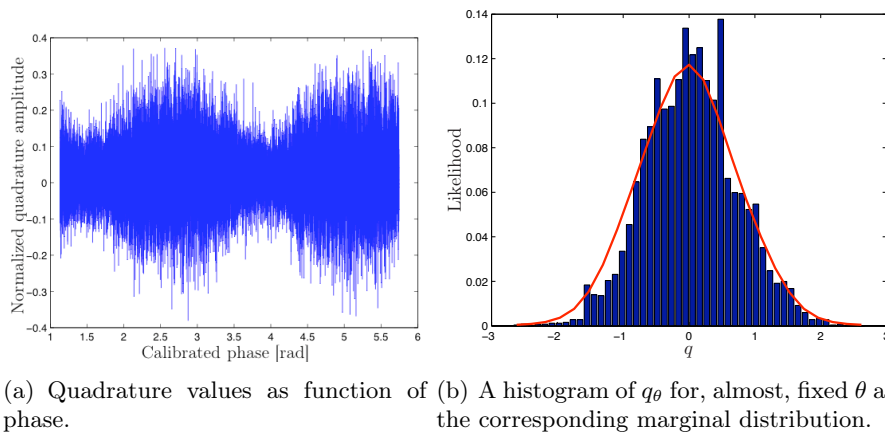


Figure 3.16: Comparing the variance in the quadrature with the marginal distribution of the Wigner function.

With this final check also yielding confirming results, we have now justified the use of the MaxLik algorithm to reconstruct the density matrix. We can thus safely conclude that the plots presented in Figure 3.14 are clearly related to the actually measured state, and that fine agreement with the theory is observed.

Chapter 4

Summary and outlook

In this chapter we will attempt to tie up any loose ends, and try to put our work into a broader perspective.

4.1 Summary

What we have witnessed is the production, measurement and reconstruction of a squeezed state of light. We have seen how a second harmonic generator can be successfully employed to provide a stable pump for the degenerate parametric down-converter. In addition to this, we have seen how the maximum likelihood algorithm can provide a faithful tool for reconstructing the quantum state of light.

As far as improvements of the setup with respect to squeezing is concerned, there is still much to be done. A squeezing of 2-3 dB is indeed no world record (see for instance [14]), and there are a lot of immediate improvements one can mention, for instance the spatial overlapping of the signal and local oscillator beams, a less noisy environment (the setup is quite sensitive to acoustic noise) and of course better photodetectors. However, the authors have felt that producing the squeezing was more a question of actually getting the quantum noise below the SQL, rather than doing a quantum limbo competition of "how low can you go" once we got there. Furthermore, the setup we used has for long been integrated in other quantum optical experiments, where the use for squeezed light is more subtle than just keeping it as quiet as possible. But, of course, more squeezing would always have been nice.

Considering the operation of the SHG, this was a success in the sense that a stable blue pump was generated for the OPO. However, many optimizations could be performed on the frequency doubler, especially does the measured conversion efficiency of around 50% seem somewhat low [13].

4.2 Outlook

Besides from just raising numbers through optimization, a really interesting point one could look into, if given more time, would be a theoretical prediction of the amount of squeezing achieved in the OPO, and its dependency on the interaction strength g . Also, it would be of interest to answer the question about what exactly it is we are squeezing, see [11] or [12].

Instead of just considering squeezing, one could also expand the squeezing setup to generate even more exotic and exciting states, for instance single photon states and Schrödinger kitten states [11]. But, as mentioned in the introduction, the field is rapidly developing, and many future applications of squeezing will certainly emerge.

Bibliography

- [1] H.-A. Bachor and T. C. Ralph. *A Guide to Experiments in Quantum Optics*. Wiley-VCH, 2004.
- [2] E. D. Black. An introduction to pound-drever-hall laser frequency stabilization. *Am. J. Phys.*, 69:79–87, 2001.
- [3] G. D. Boyd and D. A. Kleinman. Parametric interaction of focused gaussian light beams. *J. App. Phys.*, 39:3597–3639, 1968.
- [4] G. Breitenbach, S. Schiller, and J. Mlynek. Measurement of the quantum states of squeezed light. *Nature*, 387:471–475, 1997.
- [5] C. C. Gerry and P. L. Knight. *Introductory Quantum Optics*. Cambridge University Press, 2005. Reprinted with corrections 2006.
- [6] M. Hillery, R. F. O’Connell, M. O. Scully, and E. P. Wigner. Distribution functions in physics: Fundamentals. *Phys. Rep.*, 106:121–167, 1984.
- [7] U. Leonhardt. *Measuring the Quantum State of Light*. Cambridge Studies in Modern Optics. Cambridge University Press, 1997.
- [8] A. I. Lvovsky. Iterative maximum-likelihood reconstruction in quantum homodyne tomography. *J. Opt. B*, 6:S556–S559, 2004.
- [9] P. W. Milonni and J. H. Eberly. *Lasers*. John Wiley & Sons, Inc., 1988.
- [10] J. S. Neergaard-Nielsen. Nonclassical light source for quantum networks. Master’s thesis, University of Copenhagen, February 2005.
- [11] J. S. Neergaard-Nielsen. *Generation of single photons and Schrödinger kitten states of light*. PhD thesis, University of Copenhagen, July 2008.
- [12] B. M. Nielsen. Generation of a schrödinger kitten state of light. Master’s thesis, University of Copenhagen, September 2006.
- [13] Z. Y. Ou, S. F. Pereira, E. S. Polzik, and H. J. Kimble. 85 % efficiency for cw frequency doubling from 1.08 to 0.54 μm . *Optics Letters*, 17:640–642, 1992.
- [14] E. S. Polzik, J. Carri, and H. J. Kimble. Spectroscopy with squeezed light. *Phys. Rev. Lett.*, 68:3020–3023, 1992.
- [15] K. F. Riley, M. P. Hobson, and S. J. Bence. *Mathematical Methods for Physics and Engineering*. Cambridge University Press, third edition, 2006.
- [16] J. J. Sakurai. *Modern Quantum Mechanics*. Addison-Wesley, 1994.
- [17] B. E. A. Saleh and M. C. Teich. *Fundamentals of Photonics*. Wiley Series in Pure and Applied Optics. John Wiley & Sons, Inc., second edition, 2007.

Appendix A

The error function

In [15] the error function is defined as

$$\operatorname{erf}(x) = \frac{2}{\sqrt{\pi}} \int_0^x e^{-u^2} du, \quad (\text{A.0.1})$$

and it is stated that the relation between the error function and the cumulative probability³¹ function $\Phi(x)$ for the Gaussian distribution (i.e. the integrated Gaussian distribution) is

$$\begin{aligned} \Phi(x) &= \frac{1}{\sqrt{2\pi}} \int_{-\infty}^x e^{-u^2/2} du \\ &= \frac{1}{2} + \frac{1}{\sqrt{2\pi}} \int_0^x e^{-u^2/2} du \\ &= \frac{1}{2} + \frac{1}{2} \operatorname{erf}\left(\frac{x}{\sqrt{2}}\right), \end{aligned} \quad (\text{A.0.2})$$

where one has made use of the well-known Gaussian integral

$$\int_{-\infty}^{\infty} e^{-u^2/a} du = \sqrt{\frac{\pi}{a}}, \quad (\text{A.0.3})$$

as well as the evenness of the Gaussian distribution function. From (A.0.2) it is evident that the amount of light intensity measured by a photodetector as the light beam is gradually blocked will have a simple relation to the error function. This is indeed what 'the japanese swinging stick fitting algorithm' makes use of. In figure A.1 the data was fitted in gnuplot against a function of the form

$$f(x) = A * (1 - \operatorname{erf}(c * x + b)) + d. \quad (\text{A.0.4})$$

In real life Matlab is used.

³¹We cumulate intensity rather than probability, but the distribution is the same.

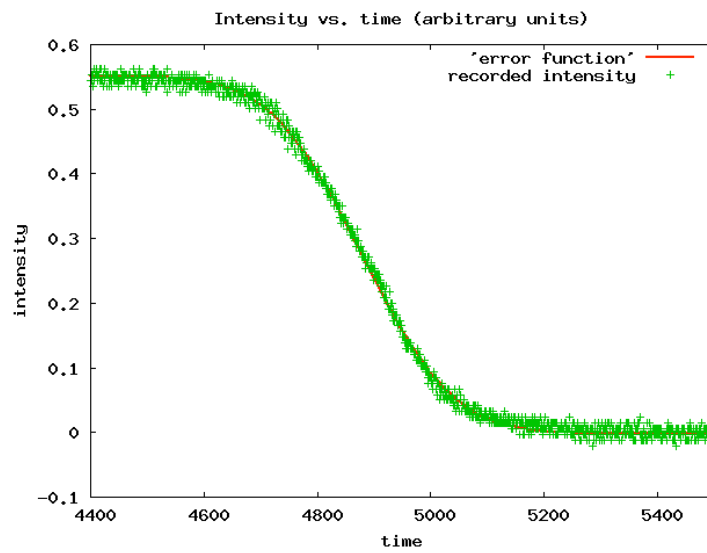


Figure A.1: A convincing relationship.

Appendix B

Lorentz model of SHG

In this Appendix we give a fully classical treatment of second harmonic generation, following [9]. This treatment, however conceptually flawed by modeling an atom as a nucleus with a billiard ball electron attached to it on a spring, is useful to us as it makes a good prediction of the phase matching condition.

B.1 Nonlinear material

The displacement of an electron, $x(t)$, in a electromagnetic field, $E(t)$, is derived in [9, section 2.3]. Taking the light to be linearly polarized in the x -direction, we have

$$\ddot{x} + \omega_0 x = \frac{e}{m} E(t), \quad (\text{B.1.1})$$

where ω_0 denotes the natural oscillation frequency of the electron. Before going on, we note that in order to obtain equation (B.1.1), we have made the assumption that the contribution from the magnetic force can be neglected since we are considering non-relativistic particles. We now make the dipole approximation, valid since an optical wavelength ($\lambda \approx 850$ nm) is much larger than the size of an atom (≈ 0.1 nm). In this approximation, the energy of a dipole, \mathbf{d} , in a electric field, is given by $\mathbf{d} \cdot \mathbf{E}(\mathbf{r}, t)$. Finally, we have approximated the real potential by a parabolic potential. The last assumption is only true as long as we consider light of low intensities, i.e. the external field in equation (B.1.1) is of low amplitude. Solving equation (B.1.1) with the mentioned approximations, one finds ³²

$$x_1 = \frac{e/m}{\omega_0^2 - \omega^2} E_0 \cos(\omega t). \quad (\text{B.1.2})$$

The approximation of a parabolic potential will, however, break down at higher intensities, since it is nothing but a second order Taylor approximation, valid only within some interval centered around the equilibrium position. To deal with larger displacements we must include higher order terms in our approximation of the potential. These higher order terms will be denoted nonlinear, for reasons that will become obvious. If we include the first nonlinear term, the equation of motion for the electron becomes

$$\ddot{x} + \omega_0 x + ax^2 = \frac{e}{m} E_0 \cos(\omega t), \quad (\text{B.1.3})$$

where we have taken $E(t) = E_0 \cos(\omega t)$. Since this is a non-linear differential equation, it is either rather challenging to solve, or in some cases unsolvable. In order

³²Note that we have neglected the homogeneous solution to equation (B.1.1), since this will damp out within any realistic relaxation time.

to simplify equation (B.1.3), we will assume that the non-linear term, ax^2 , is small. With this we can treat the nonlinear term as a perturbation of the linear equation. Obviously, the first order approximation, neglecting the nonlinear term, just gives us the linear oscillator model. Going to second order, we set $ax^2 \approx ax_1^2$, inserting and solving for the displacement in equation (B.1.3) yields

$$x_2(t) = x_0 + \frac{1}{2} [x_\omega e^{-i\omega t} + x_\omega^* e^{i\omega t}] + \frac{1}{2} [x_{2\omega} e^{-2i\omega t} + x_{2\omega}^* e^{2i\omega t}], \quad (\text{B.1.4})$$

where

$$\begin{aligned} x_0 &= -\frac{a}{2\omega_0^2} \left(\frac{e/m}{\omega_0^2 - \omega^2} \right)^2 |\mathcal{E}_\omega|^2 \\ x_\omega &= \frac{e/m}{\omega_0^2 - \omega^2} \mathcal{E}_\omega \\ x_{2\omega} &= -\frac{a}{2} \frac{1}{\omega_0^2 - 4\omega^2} \left(\frac{e/m}{\omega_0^2 - \omega^2} \right)^2 \mathcal{E}_\omega^2. \end{aligned} \quad (\text{B.1.5})$$

Since the polarization, P , is proportional to the electron displacement given in equation (B.1.3), we find polarization terms at frequencies ω and 2ω . From Maxwell's equations in dielectric media, it follows that

$$\nabla^2 E - \epsilon_0 \mu_0 \frac{\partial^2 E}{\partial t^2} = \mu_0 \frac{\partial^2 P}{\partial t^2}. \quad (\text{B.1.6})$$

Since this is a linear equation we see that the polarization oscillating at 2ω will induce an electric field at the same frequency. Within the framework of this classical theory, we are now ready to arrive at the main result, namely an expression for the field at 2ω .

If we assume a monochromatic plane wave as input field, the field $\mathcal{E}_{2\omega}$ to be slowly varying³³ in z compared with $e^{ik_{2\omega}z}$ and that the pump field is nondepleted by the second harmonic generation, i.e. $\mathcal{E}_\omega(z) \approx \mathcal{E}_\omega(0)$ (this last assumption obviously puts some unfortunate constraints on our expected efficiency!), one finds

$$\mathcal{E}_{2\omega}(\ell) = i\omega \sqrt{\frac{\mu_0}{\epsilon_{2\omega}}} \bar{d} \mathcal{E}_\omega^2(0) \ell e^{\Delta k \ell / 2} \frac{\sin\left(\frac{1}{2} \Delta k \ell\right)}{\frac{1}{2} \Delta k \ell}, \quad (\text{B.1.7})$$

where we have introduced the wave vector mismatch, $\Delta k = 2k_\omega - k_{2\omega}$, and the material dependent tensor \bar{d} ³⁴. The intensity (averaged over time) in terms of the complex amplitude is given as

$$I = \frac{1}{2} \sqrt{\frac{\epsilon_0}{\mu_0}} |\mathcal{E}|^2, \quad (\text{B.1.8})$$

thus for the frequency doubled field after it has passed through a crystal of length ℓ we have

$$I_{2\omega}(\ell) = 2 \left(\frac{\mu_0}{\epsilon_0} \right)^{3/2} \frac{\omega^2 \bar{d}^2}{n^2(\omega) n(2\omega)} I_\omega(0)^2 \ell^2 \left(\frac{\sin\left(\frac{1}{2} \Delta k \ell\right)}{\frac{1}{2} \Delta k \ell} \right)^2. \quad (\text{B.1.9})$$

The sinc² function has now been justified.

³³This is indeed no cruel approximation, as it only amounts to assuming $\mathcal{E}_{2\omega}$ constant over a few optical cycles. See [9, p. 250].

³⁴The reader can either simply accept the poor definition given here, or consult [9, Section 17.13] or [10, Page 19] and the references herein.

Appendix C

Derivation of the Gaussian beam

C.1 The paraxial wave equation

Taking a monochromatic plane wave, $E(\mathbf{r}, t) = \mathcal{E}(\mathbf{r})e^{-i\omega t}$ and inserting into the wave equation given by

$$\nabla^2 \mathcal{E} - \frac{1}{c^2} \frac{\partial^2 \mathcal{E}}{\partial t^2} = 0 \quad (\text{C.1.1})$$

one obtains the Helmholtz equation for the complex amplitude $\mathcal{E}(\mathbf{r})$:

$$\nabla^2 \mathcal{E}(\mathbf{r}) - k^2 \mathcal{E}(\mathbf{r}) = 0 \quad (\text{C.1.2})$$

As stated above, (3.2.1) and (3.2.2) are two solutions hereof. We take the direction of propagation to be along the z -axis and modify our plane wave in accordance with the approximation that the amplitude varies slowly on the scale of a wavelength, which seems reasonable for optical laser beams. We write this as

$$\lambda \left| \frac{\partial \mathcal{E}}{\partial z} \right| \ll |\mathcal{E}|, \quad \lambda \left| \frac{\partial^2 \mathcal{E}}{\partial z^2} \right| \ll \left| \frac{\partial \mathcal{E}}{\partial z} \right|. \quad (\text{C.1.3})$$

This approximation allows us to neglect several terms as we insert the plane wave $\mathcal{E}(\mathbf{r}) = \mathcal{E}_0(\mathbf{r})e^{ikz}$ into the Helmholtz equation. What we obtain is the paraxial wave equation³⁵ (also known as the paraxial Helmholtz equation)

$$\nabla_T^2 \mathcal{E}_0 + 2ik \frac{\partial \mathcal{E}_0}{\partial z} = 0, \quad (\text{C.1.4})$$

where ∇_T^2 is the transverse Laplacian defined as (w. propagation along the z -axis)

$$\nabla_T^2 = \frac{\partial^2}{\partial x^2} + \frac{\partial^2}{\partial y^2}. \quad (\text{C.1.5})$$

A simple solution hereof is the so-called paraboloidal wave [17, Page 76], which has the amplitude

$$\mathcal{E}_0(\mathbf{r}) = \frac{C}{z} \exp \left[ik \frac{\rho^2}{2z} \right], \quad \rho^2 = x^2 + y^2, \quad (\text{C.1.6})$$

where C is some constant. We note the encouraging features that the intensity gets 'smeared out' over a larger cross-sectional area as the beam propagates, and that the intensity distribution in this transverse plane is cylindrically symmetric, two features that are readily observed with real-life laser beams. The Gaussian beam is now to be obtained from (C.1.6) by the shift in variables $z \rightarrow z - \zeta$, and choosing ζ to be purely imaginary, say, $\zeta = iz_0$.

³⁵Note the similarity between this and the Schrödinger equation.